FRANC3D & BES

Benchmarking

Version 2.6

2003

1 Introduction

FRANC3D/BES is capable of evaluating stress intensity factors (SIFs) along three-dimensional crack fronts and then propagating these cracks. It is necessary to have accurate SIFs before the propagation can be validated. This document verifies FRANC3D's ability to compute SIFs accurately. Propagation is then validated through comparison with results from some previous experimental and other numerical studies. The stress analysis required to compute SIFs is performed with the 3D boundary element program, BES [Lutz, 1991].

2 SIF Verification

Several models are used to compare predictions from FRANC3D to handbook or analytical solutions. For each model, several mesh densities are created, and three different element types are used with each mesh. The element types include all linear elements, all quadratic with quarter-point crack front elements, and all linear except for quarter-point elements along the crack front. The solution time rapidly increases with the number of elements on the crack surface. Also, the solution time for all quadratic elements is much greater than the solution time for all linear elements. Using quadratic quarter-point elements along the crack front only slightly increases the solution time compared to the use of all linear elements.

SIFs are computed using the displacement correlation technique for all cases [Chan *et al.*, 1970]. Either the first row of mesh nodes behind the crack front, Figure 1, or points located a constant distance, r , from and evenly spaced along the geometric crack front, Figure 2, are used as locations for computing crack (opening and sliding) displacements (CODs, CTDs, and CSDs) and SIFs. The values for the two sets of points are generally close; however, sometimes one method gives a smoother variation depending on the crack front curvature and the mesh density. A third option is available, using points at mid-points of the crack front mesh edges.

The SIFs are recorded in tables for each model. The value for each mesh and element scheme is compared to the handbook or analytical solution and the percentage error is recorded for each value. The percentage error is computed as the absolute difference between the computed and handbook/analytical value, divided by the handbook/analytical value, and multiplied by 100.

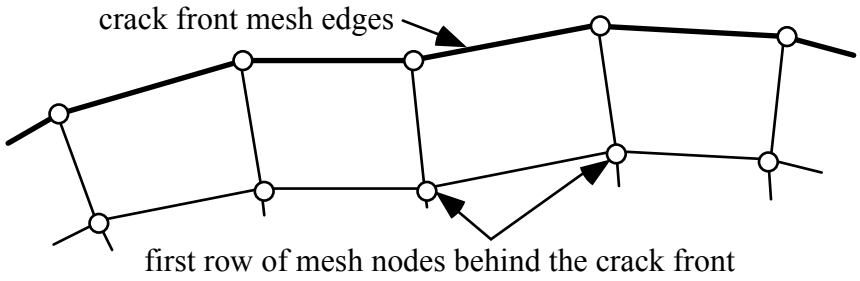

Figure 1. The first row of mesh nodes behind the crack front can be used as the locations for computing crack displacements and stress intensity factors.

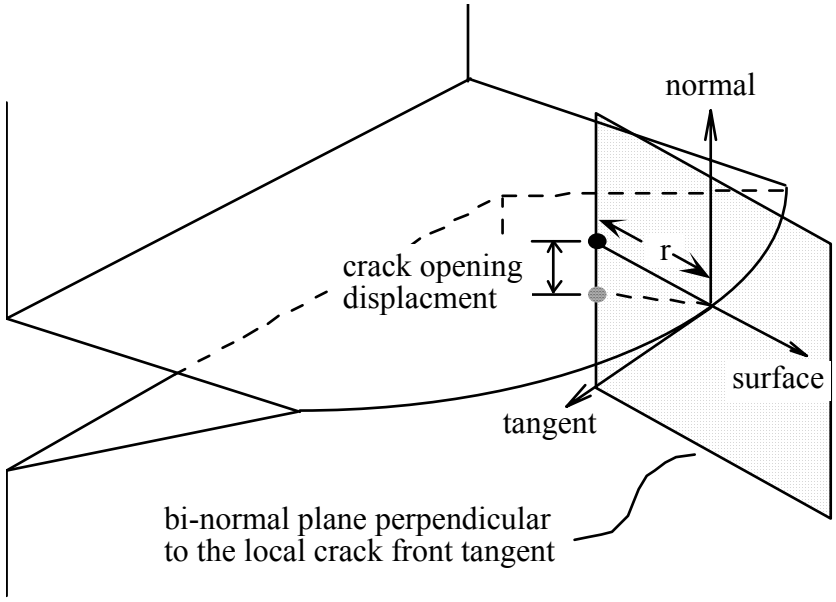

Figure 2. Crack displacements can be computed at a measured distance from the geometric crack front edges to determine the stress intensity factors.

2.1 Example 1: Plate with a Single, Flat, Part-Through Edge Crack

Figure 3 shows a model of a plate with a single, flat, part-through edge crack. Six elements are used through the thickness of the plate, that is, along the crack front. An increasing number of elements is used along the crack length, Figure 4, starting with a single element and increasing to 24 elements to examine the effect of mesh refinement. The remainder of the mesh on the plate surfaces remains the same, except for the surfaces adjacent to the crack edges; these must be refined as the number of subdivisions along the crack edges change. The loading on the plate is uniform tension equal to 1.0, and material properties include an elastic modulus of 10,000, and a Poisson's ratio of 0.0 so that the solution can be compared to the available 2D handbook answer.

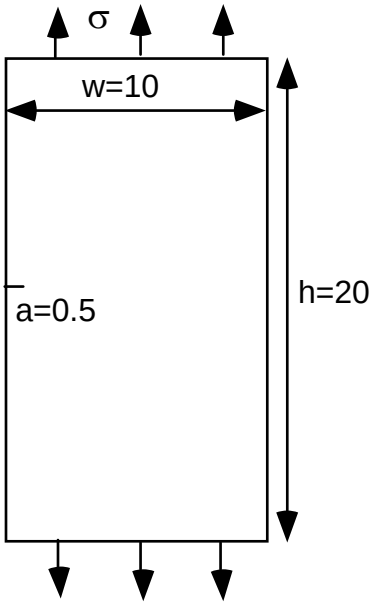

Figure 3. Example 1: Single edge crack model under remote tension.

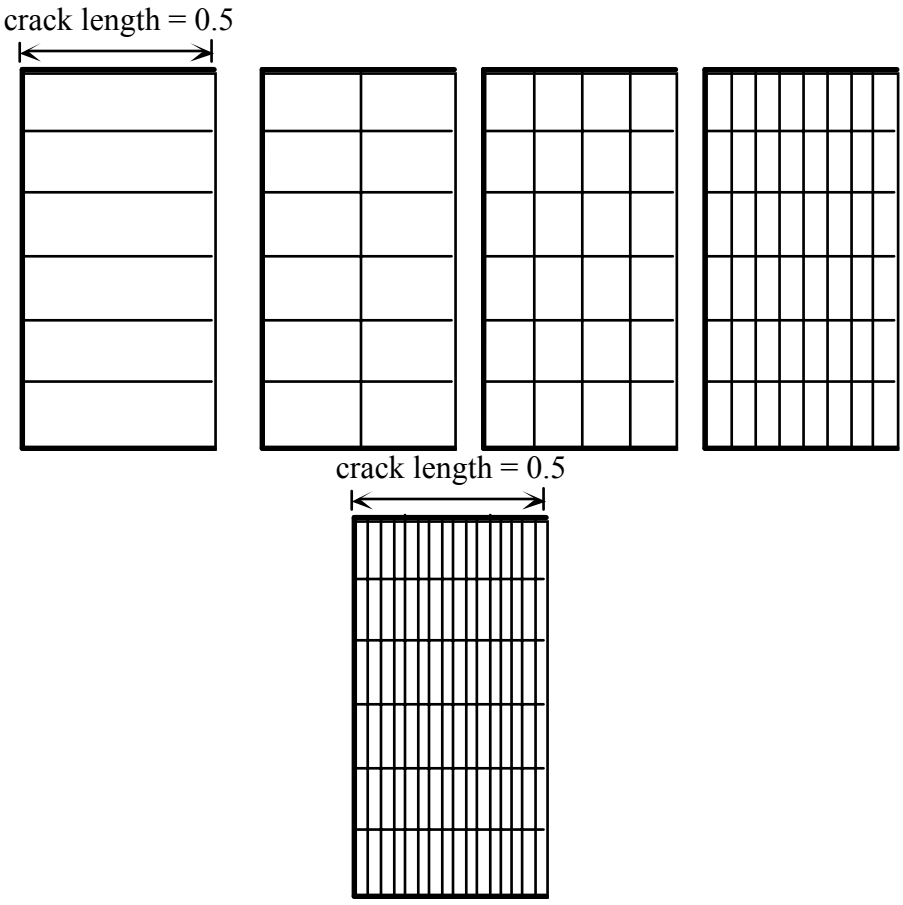

Figure 4. Example 1: Details of mesh models along the crack (mesh with 24 subdivision along the crack length is not shown).

The handbook solution for Mode I SIF for an edge crack in a finite plate is given in Murakami (Ref. 3, page 9) as:

$$K_I = \sigma\sqrt{\pi a} \quad F_I(\alpha)$$

The correction factor is:

$$\alpha = \frac{a}{w}$$

$$F_I(\alpha) = \left(1.12 - 0.231\alpha + 10.55\alpha^2 - 21.72\alpha^3 + 30.39\alpha^4\right)$$

for $a/w \le 0.6$. $K_{II} = K_{III} = 0$

For the plate and crack dimensions above, the correction factor is 1.132, which gives a value for K_I of 1.419 for this example. This value is accurate to within 0.5%.

This value is compared with that predicted by FRANC3D for a fully 3D model of unit thickness. To avoid the boundary effects as much as possible, the first and last value of stress intensity factor along the crack front are removed and the remaining five values are averaged. Table 1a summarizes the results. The SIF is underestimated with a coarse mesh consisting of a single element along the crack length. As the mesh is refined, the handbook SIF is approached, and then overestimated.

Table 1a: Mode I SIF values averaged along the crack front for increasing number of elements along the crack length, and the three element types, for Example 1.

Model File Name	All Linear	% error	All Quadratic	% error	Quadratic Front	% error
Handbook	**1.419**	+/- 0.5				
ex1_m1x6	1.149	19.0	1.366	3.7	1.270	10.5
ex1_m2x6	1.365	3.8	1.506	6.1	1.481	4.4
ex1_m4x6	1.451	2.2	1.557	9.7	1.565	10.3
ex1_m8x6	1.483	4.5	1.584	11.6	1.603	12.9
ex1_m16x6	1.493	5.2	1.590	12.0	1.620	14.1
ex1_m24x6	1.492	5.1	1.584	11.6	1.622	14.2

The SIF values converge as the mesh is refined, but they converge to a values greater than the handbook solution. It should be noted that the FRANC3D SIF is higher near the free surface ("crack tip") than in the middle of the crack front. To investigate the effect of the free surface on the SIF value, the mesh is refined in the through-thickness direction. Using the second, third and fourth meshes of Figure 4, the number of elements along the crack front is increased from 6 to 8, 12, and 16. Only linear elements are used with these meshes. The average Mode I SIF values, discarding the first and last values again, are given in Table 1b. It is quite clear that the solution converges to the handbook solution as the number of elements increases in both directions. The free surface has a significant effect on the computed value, and it is clearly necessary to use *enough* elements in both along the crack length and along the crack front to obtain a reasonable answer. It is possible to obtain very accurate values with a fairly coarse mesh (of 4 by 12 elements for this example model), but, in general, a user must refine the mesh in both directions to get proper convergence.

Table 1b: Mode I SIF values averaged along the crack front for increasing number of elements along the crack front for the second, third and fourth meshes of Figure 4 of Example 1.

Model File Name	All Linear	% error	Model File Name	All Linear	% error	Model File Name	All Linear	% error
Handbook	**1.425**	+/- 0.5	**Handbook**	**1.425**	+/- 0.5	**Handbook**	**1.425**	+/- 0.5
ex1_m2x6	1.365	4.2	ex1_m4x6	1.451	2.6	ex1_m8x6	1.483	5.8
ex1_m2x8	1.341	5.9	ex1_m4x8	1.441	1.1	ex1_m8x8	1.482	4.0
ex1_m2x12	1.331	6.6	ex1_m4x12	1.432	0.5	ex1_m8x12	1.474	3.5
ex1_m2x16	1.324	7.1	ex1_m4x16	1.426	0.07	ex1_m8x16	1.432	0.5

2.2 Example 2: Single, Internal, Flat, Penny-Shaped Crack

Figure 5 shows a model of an infinite body with an internal penny-shaped crack with a radius of 0.1. This crack is centered in a block with dimensions 10 x 5 x 5 in the FRANC3D/BES model. Six elements are used along each quarter of the circumference of the crack for the first two models, 8 elements are used for the third, and 12 elements are used for the fourth model, Figure 6. The number of elements along the radius increases from an initial value of 2, to 3, to 8, to a final value of 12. The loading is a far-field, uniform, unit tension normal to the crack surface. The material properties consist of an elastic modulus of 10,000 and a Poisson's ratio of 0.0.

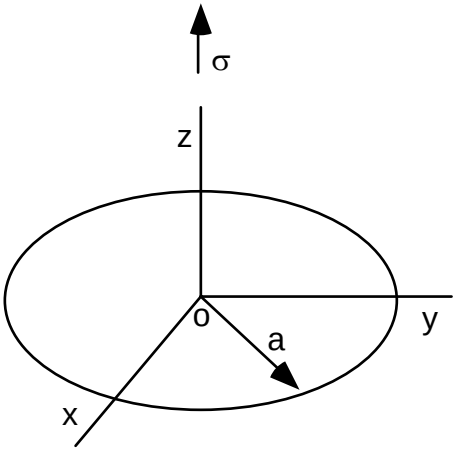

Figure 5. Example 2: Flat, internal, penny-shaped crack subjected to remote tension.

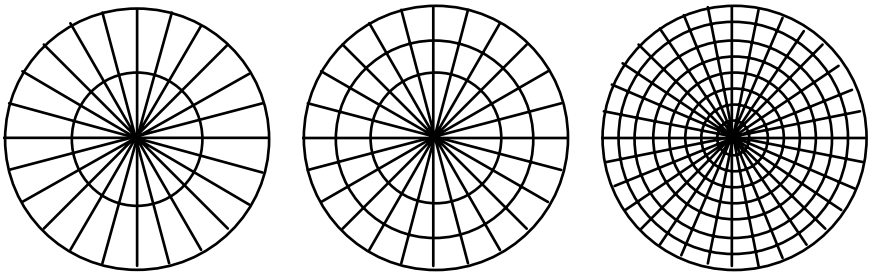

Figure 6. Example 2: Meshes for models 1, 2 and 3 (mesh 4 with 12 subdivisions along each quarter of the crack front and 12 subdivisions along the radius is not shown).

The analytical solution for the Mode I SIF for such a crack is given by Sneddon (see Murakami, page 668, Ref. 3) as:

$$K_I = 2\,\sigma\sqrt{\frac{a}{\pi}}$$

$$K_{II} = K_{III} = 0$$

There is no correction factor required, so the target value of K_I is 0.357, constant around the crack front. The Mode I SIF's from FRANC3D/BES are determined by averaging all the values along the crack front. The average SIFs are given in Table 2. The SIF is underestimated with the coarser meshes. As the mesh is refined, it is overestimated, at least when using quadratic elements.

Table 2: Average Mode I SIF values for increasing number of elements along the radius and the three element schemes, Example 2.

Model File Name	All Linear	% error	All Quadratic	% error	Quadratic Front	% error
Analytical	**0.357**					
ex2_m2x6	0.299	16.3	0.321	10.2	0.329	7.9
ex2_m3x6	0.331	7.1	0.345	3.2	0.357	0.0
ex2_m8x8	0.342	4.1	0.355	0.4	0.368	3.1
ex2_m12x12	0.348	2.6	0.363	1.6	0.374	4.9

2.3 Example 3: Single, Internal, Flat, Elliptical Crack (Aspect Ratio 1:2)

Figure 7 shows a model of an infinite body with an internal, flat, elliptical crack with an aspect ratio of 1:2. A crack with a minor axis of 0.10 and major axis of 0.20. is centered in a block with dimensions 10 x 5 x 5 in the FRANC3D/BES model. Twelve elements are used along each quarter of the perimeter for all models. Four different meshes are used; the first has elements that increase in length when going from the minor to the major axis, the third has a row of elements that are roughly all the same length along the crack front perimeter, Figure 7. The second is a refined version of the first, and the fourth is a refined version of the third. The first and third meshes use three elements along the major and minor axes, the second and fourth meshes use five.

The loading is far-field uniform tension equal to 1.0 and the material properties consist of an elastic modulus of 10,000 and a Poisson's ratio of 0.0.

The analytical values for Mode I, II and III SIFs are available from Kassir and Sih (see Murakami page 684, Ref. 3) for arbitrary loading, aspect ratios, and crack orientations. For a flat, elliptical crack with remote tension normal to the crack surface, the Mode II and III SIFs are zero everywhere along the crack front. Mode I SIFs vary along the crack front perimeter with a maximum value of 0.463 at the end of the minor axis, and a minimum value of 0.327 at the end of the major axis. The equations involve elliptic integrals and have been encoded into a computer program so that we can compare the analytical values with the numerical values. The maximum and minimum values of K_I for the four meshes and the three different integration schemes are recorded in Table 3 and 4 respectively.

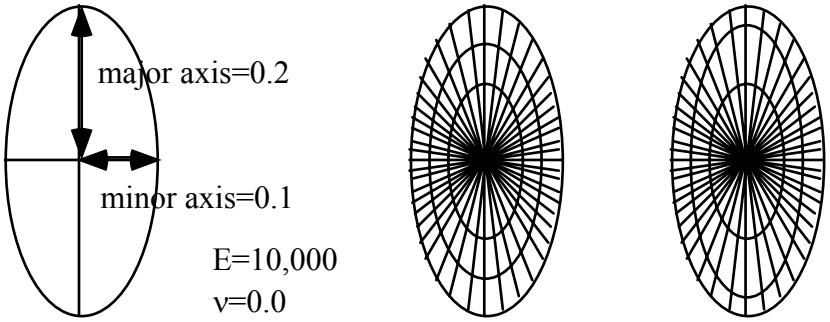

Figure 7. Example 3: Elliptical crack shape and the meshes 1 and 3. The meshes 2 and 4 are refined versions of these meshes with five elements along each axes.

Table 3: Maximum values of Mode I SIF for the four meshes and the three element types, Example 3. Note the NR indicates that the BES analysis was not run.

Model File Name	All Linear	% error	All Quadratic	% error	Quadratic Front	% error
Analytical	**0.463**					
ex3_m3x12a	0.427	7.8	0.449	3.0	0.462	0.2
ex3_m5x12a	0.435	5.9	NR	---	0.471	1.7
ex3_m3x12b	0.455	1.2	NR	---	0.470	1.5
ex3_m5x12b	0.425	8.1	NR	---	0.464	0.2

Table 4: Minimum values of Mode I SIF for the four meshes and the three element types, Example 3. Note the NR indicates that the BES analysis was not run.

Mesh Model	All Linear	% error	All Quadratic	% error	Quadratic Front	% error
Analytical	**0.327**					
ex3_m3x12a	0.295	9.8	0.316	3.3	0.321	1.8
ex3_m5x12a	0.304	7.0	NR	---	0.329	0.5
ex3_m3x12b	0.346	5.9	NR	---	0.346	5.6
ex3_m5x12b	0.315	3.6	NR	---	0.340	3.7

2.4 Example 4: Single, Internal, Inclined (45 degrees), Penny-Shaped Crack

A 10x5x5 block is used to model an infinite body containing a centered, internal, penny-shaped crack of radius 0.125, inclined at 45 degrees, Figure 8. The loading is far-field uniform tension equal to 1.0 and the material properties consist of an elastic modulus of 10,000 and a Poisson's ratio of 0.0. The first model use six elements along each quarter of the crack front perimeter, the second and third use eight, and the fourth model uses twelve. Along the radius, 2, 4, 6, and 8 elements are used for the first, second, third and fourth model, respectively (the meshes are similar to those shown in Figure 6).

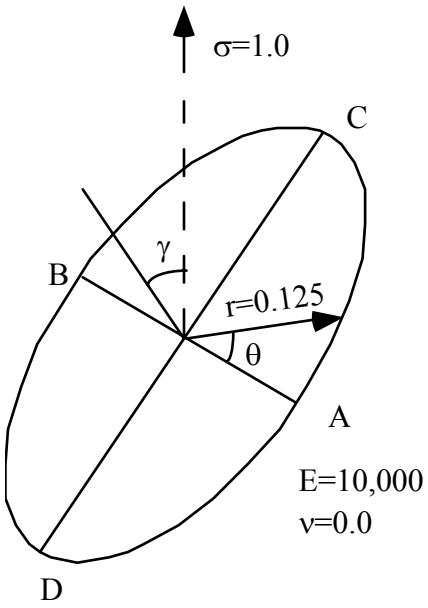

Figure 8. Example 4: Inclined, penny-shaped crack subjected to uniform, remote tension.

The analytical values for Mode I, II and III SIFs are available in Murakami (Ref. 3, page 684). Mode I SIF is constant at 0.200 along the crack front perimeter. The Mode II SIF is zero at the points A and B, Figure 8, and reaches a maximum (or minimum depending on the sign) at points C and D equal to 0.200. Mode III SIF is zero at points C and D, and reaches a maximum at points A and B equal to 0.200. The equations for the three modes of SIF are:

$$K_I = \sigma \sin^2(\gamma)\sqrt{\pi r}\,(2/\pi)$$

$$K_{II} = \sigma \sin(\gamma)\cos(\gamma)\sin(\theta)\sqrt{\pi r}\,(2/\pi)(2/(2-\nu))$$

$$K_{III} = \sigma \sin(\gamma)\cos(\gamma)\cos(\theta)\sqrt{\pi r}\,(2/\pi)(2/(2-\nu))(1-\nu)$$

where γ is the angle of inclination (here 45 degrees), θ is the position along the crack front, r is the crack radius, and ν is the Poisson's ratio.

In Tables 5, 6 and 7, we compare the analytical values with the average value for K_I, and the maximum values of K_{II} and K_{III} for the four different meshes and the three element types.

Table 5: Average values of Mode I SIF for the four meshes and the three element types, Example 4. Note the NR indicates that the BES analysis was not run.

Model File Name	All Linear	% error	All Quadratic	% error	Quadratic Front	% error
Analytical	**0.200**					

ex4_m2x6	0.165	17.5	NR	---	0.183	8.3
ex4_m4x8	0.193	3.5	0.197	1.5	0.208	4.0
ex4_m6x8	0.195	2.5	0.202	1.0	0.209	4.5
ex4_m8x12	0.191	4.5	NR	---	0.206	3.0

Table 6: Maximum values of Mode II SIF for the four meshes and the three element types, Example 4. Note the NR indicates that the BES analysis was not run.

Model File Name	All Linear	% error	All Quadratic	% error	Quadratic Front	% error
Analytical	**0.200**					
ex4_m2x6	0.165	17.5	NR	---	0.183	8.3
ex4_m4x8	0.192	4.0	0.200	0.0	0.206	3.0
ex4_m6x8	0.194	3.0	0.201	0.5	0.208	4.0
ex4_m8x12	0.191	4.5	NR	---	0.206	3.0

Table 7: Maximum values of Mode III SIF for the four meshes and the three element types, Example 4. Note the NR indicates that the BES analysis was not run.

Model File Name	All Linear	% error	All Quadratic	% error	Quadratic Front	% error
Analytical	**0.200**					
ex4_m2x6	0.165	17.5	NR	---	0.183	8.3
ex4_m4x8	0.192	4.0	0.199	0.5	0.207	3.5
ex4_m6x8	0.194	3.0	0.201	0.5	0.209	4.5
ex4_m8x12	0.191	4.5	NR	---	0.206	3.0

2.5 Example 5: Single, Internal, Inclined (45 degrees), Elliptical Crack (Aspect Ratio 1:2)

A block 10x5x5 is used to model an infinite body with a centered, internal, elliptical crack with an aspect ratio of 1:2, inclined at 45 degrees. The minor axis, A-B in Figure 8, is 0.125 and the major axis, C-D, 0.25. The loading is far-field uniform tension equal to 1.0 and the material properties consist of an elastic modulus of 10,000 and a Poisson's ratio of 0.0. Twelve elements are used along each quarter of the perimeter for all models. Only two different meshes are used; one (a) has elements that increase in length when going from the minor to the major axis, the other (b) has a row of elements that are roughly all the same size along the crack front. Both meshes use three elements along the major and minor axes. The meshes are similar to those shown in Figure 7.

The analytical values for Mode I, II and III SIFs are available from Kassir and Sih (see Murakami, page 684, Ref. 3). Mode I SIF varies along the crack front with a maximum value of 0.259 at the points A and B, and a minimum value of 0.183 at points C and D. The Mode II SIF is zero at points A and B, and reaches a maximum (or minimum depending on the sign) at points C and D equal to 0.183. Mode III SIF is zero at points C and D, and is maximum at points A and B equal to 0.259. The equations involve elliptic integrals and have been encoded into a small computer program so that we can compare the analytical values with the numerical values. The maximum and minimum values of K_I as well as the maximum values for K_{II} and K_{III} for the two different meshes and the three different integration schemes are recorded in Tables 8, 9, 10, and 11.

Table 8: Minimum values of Mode I SIF for the two meshes and the three element types, Example 5.

Model File Name	All Linear	% error	All Quadratic	% error	Quadratic Front	% error
Analytical	**0.183**					
ex5_m3x12a	0.182	0.5	0.182	0.5	0.186	1.7
ex5_m3x12b	0.191	4.4	0.188	2.7	0.195	6.6

Table 9: Maximum values of Mode I SIF for the two meshes and the three element types, Example 5.

Model File Name	All Linear	% error	All Quadratic	% error	Quadratic Front	% error
Analytical	**0.259**					
ex5_m3x12a	0.262	1.3	0.258	0.3	0.267	3.2
ex5_m3x12b	0.256	1.1	0.256	1.1	0.264	2.0

Table 10: Maximum values of Mode II SIF for the two meshes and the three element types, Example 5.

Model File Name	All Linear	% error	All Quadratic	% error	Quadratic Front	% error
Analytical	**0.183**					
ex5_m3x12a	0.179	2.2	0.180	1.6	0.186	1.7
ex5_m3x12b	0.188	2.7	0.186	1.7	0.192	4.9

Table 11: Maximum values of Mode III SIF for the two meshes and the three element types, Example 5.

Model File Name	All Linear	% error	All Quadratic	% error	Quadratic Front	% error
Analytical	**0.259**					
ex5_m3x12a	0.262	1.3	0.258	0.3	0.267	3.2
ex5_m3x12b	0.256	1.1	0.256	1.1	0.264	2.0

2.6 Example 6: Circumferential Crack in a Round Bar

A solid round bar shown in Figure 9 containing a mid-height, circumferential crack of depth 1 was created along with a quarter-symmetry model with the same dimensions. The loading is far-field uniform tension normal to the crack surface and is equal to 1.0. The material properties consist of an elastic modulus of 1.0 and a Poisson's ratio of 0.3. Two meshes are used with each model. For the first mesh for both full and quarter-symmetry models, 8 elements are used along the crack front and 2 elements are used along the radius, Figure 10. For the second mesh of the full model, twelve elements are used along each quarter of the circular crack front, and four elements are used along the radius. For the second mesh of the quarter model, 24 elements are used along the crack front and five elements are used along the radius. The two models are used to show the effect of the boundary surface when modeling symmetric problems.

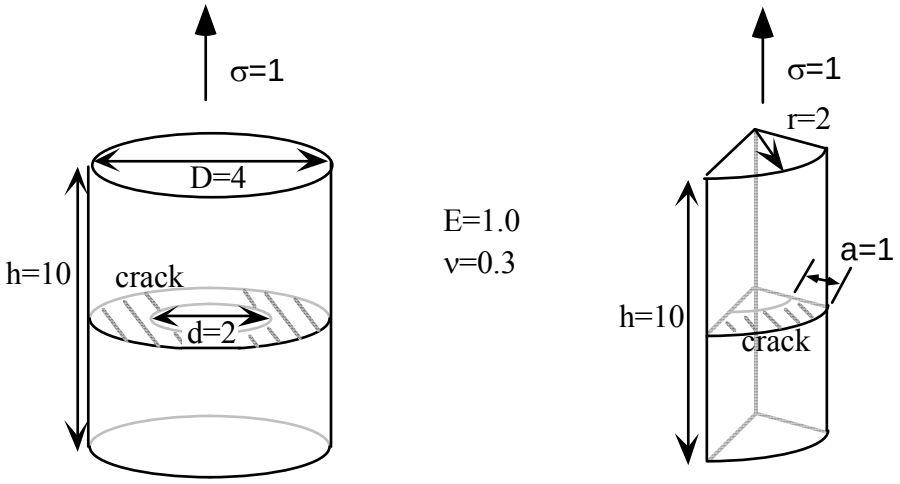

Figure 9. Example 6: Circumferentially cracked bar; full and quarter models.

The handbook solution for the Mode I SIF for this type of crack is given in Murakami (Ref 3, page 643) as

$$F_I^* = \frac{K_I}{0.5\sigma_{net}\sqrt{\pi d/2}}$$

$$\sigma_{net} = \left(\frac{D}{d}\right)^2 \sigma$$

For the bar and crack dimensions given above, the correction factor F_I^* for a Poisson ratio of 0.3 is taken from the graph in Murakami to be 0.97, which then gives a value for K_I of 3.439. This value is thought to be accurate to within 0.1%. K_{II} and K_{III} are both zero along the entire crack front. The Mode I value is compared with the average value predicted by FRANC3D/BES for both of the 3D models. The average SIF values are given in Table 12. For the quarter-symmetry model, the first and last SIF values are discarded before averaging to remove some of the boundary effects.

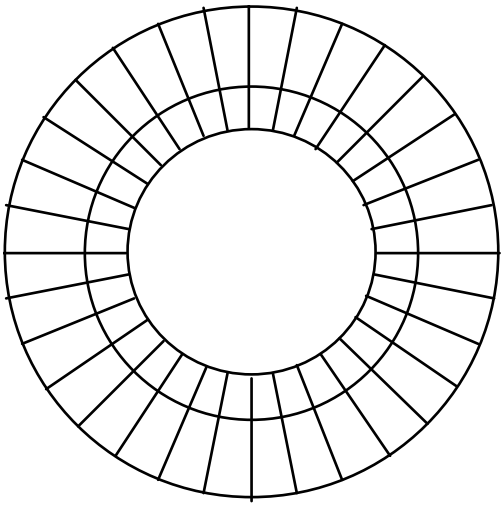

Figure 10. Example 6: First mesh for the circumferential crack in the full-bar model. The mesh for the quarter-bar model consists of one quarter of this mesh. The second mesh for both models uses both quadrilateral and triangular elements.

Table 12: Average Mode I SIF values for both the full and quarter models for the two meshes, Example 6.

Model File Name	All Linear	% error	Model File Name	All Linear	% error
Handbook	**3.439**	+/- 0.1			
ex6_m2x8_full	3.156	8.2	ex6_m2x8_qrtr	3.203	6.9
ex6_m4x12_full	3.384	1.6	ex6_m5x24_qrtr	3.361	5.0

The effect of model boundaries on the computation of the SIFs can be seen from the plot of Mode I SIF for the 2x8 meshes of both models. Figure 11 shows the SIFs along the entire crack front for the quarter-symmetry model including the values at the symmetry

surfaces. These values can be compared to those for a quarter of the crack front from the full-bar model. Note that the SIF is substantially lower at the symmetry surfaces, but is then somewhat higher for the rest of the crack front.

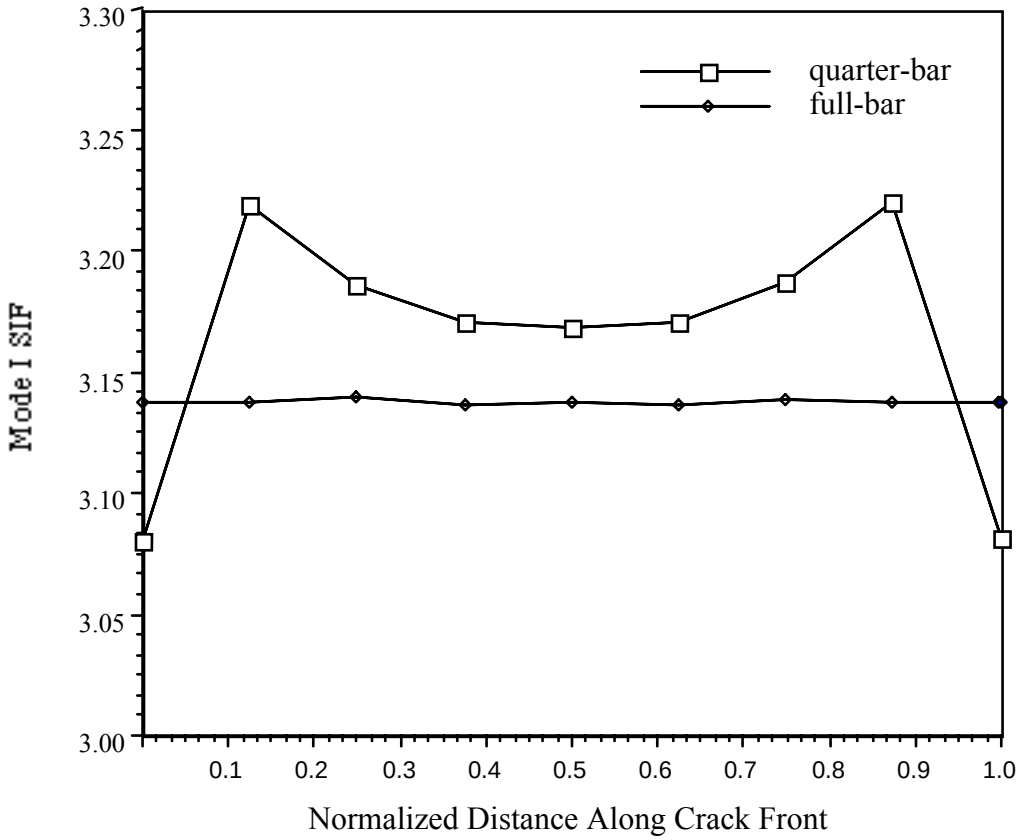

Figure 11. Example 6: Mode I SIF along a quarter of the crack front for the full-bar model and along the entire crack front for the quarter-bar model; the results are based on the first mesh for both models, i.e., 8 elements along the front and two elements along the radius.

2.7 Example 7: Half Penny-Shaped, Transverse Crack on the Inner Surface of a Pipe

Figure 12a shows the geometry of an internally cracked pipe. A half-symmetry model, Figure 12b, was also created to examine the effect of boundary surfaces when modeling problems with symmetry. A half-penny shaped, transverse crack with a radius of 0.08 is placed in the pipe on the interior surface, centered with respect to the pipe length. The material properties include an elastic modulus of 1.0e7 and Poisson's ratio of 0.33. The

loading is axial, uniform remote tension normal to the crack surface and equal to 1.0. For the full model, 36 elements were used along the crack front and for the half-symmetry model 30 elements were used. About ten elements were used along the radius for both models (triangular elements were used for part of the mesh on the crack surface).

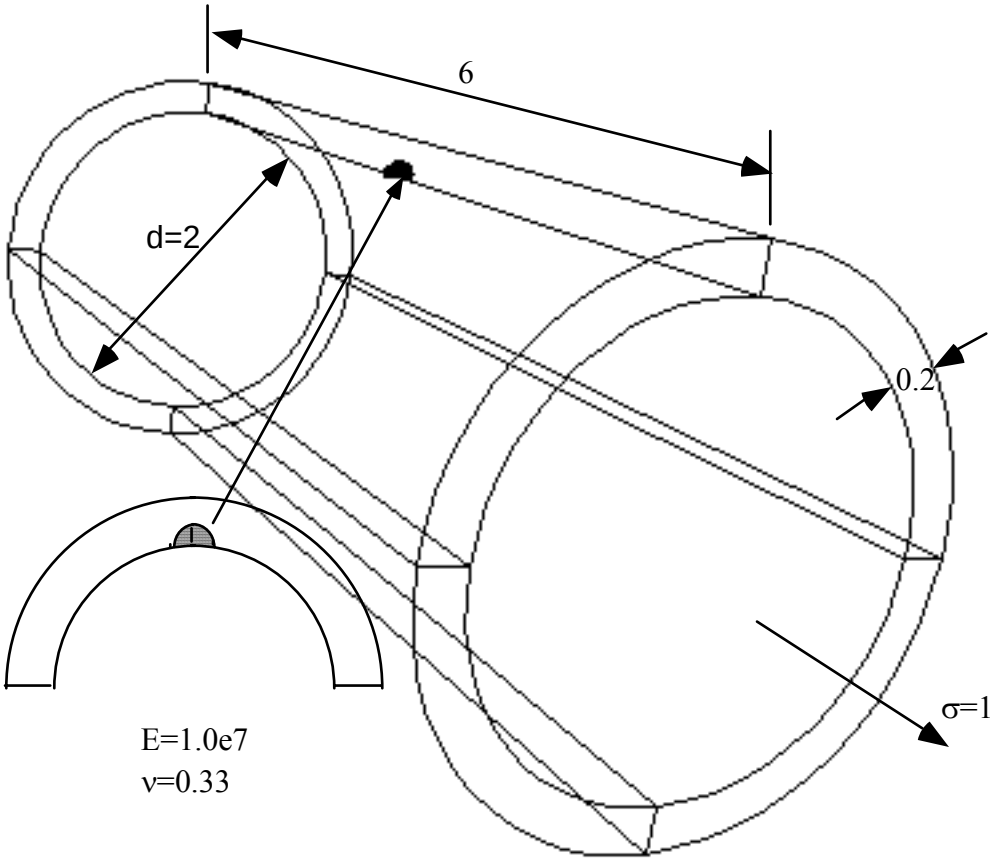

Figure 12a. Example 7: Full pipe model with transverse crack on the inner surface.

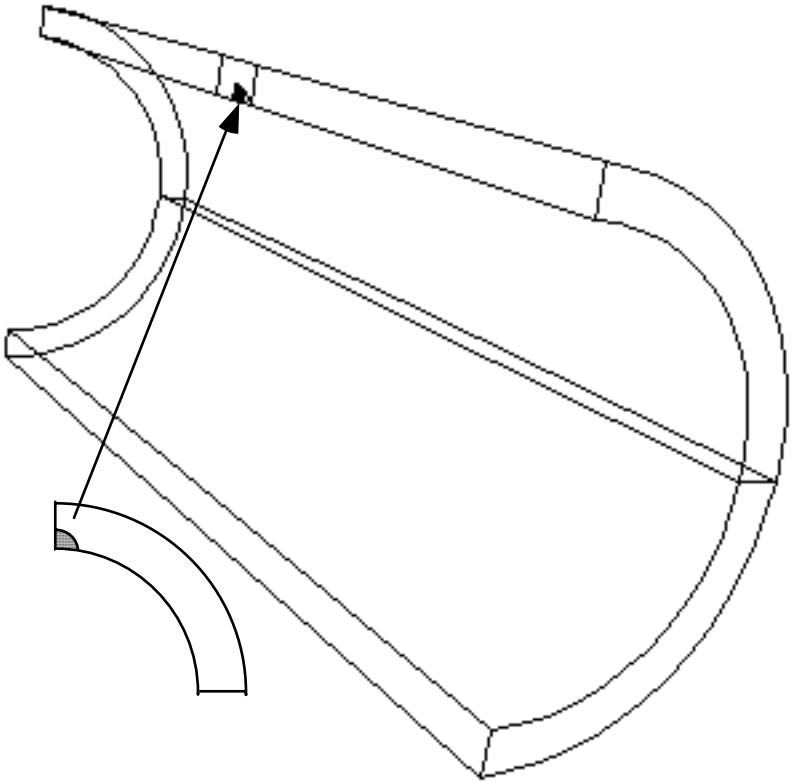

Figure 12b. Example 7: Half-symmetry model with transverse crack on the inner surface. All other dimensions, properties, and boundary conditions are identical to those for the full pipe model.

The handbook solution is available from several sources, eg.Ref. 4. The Mode II and III SIFs are zero. The minimum value of the mode I SIF occurs at the deepest part of the crack and is equal to 0.341, while the maximum occurs where the crack front meets the inner pipe surface and is equal to 0.388. The accuracy of these values is unknown: they are the result of 3D finite element analysis. The handbook solution is compared with that predicted by FRANC3D/BES in Tables 13 and 14. The SIF values are obtained at the mid-points of elements along the crack front.

Table 13: Minimum Mode I SIF values for the two models, Example 7.

Model File Name	All Linear	% difference	Model File Name	All Linear	% difference
Handbook	0.341			0.341	
ex7_m10x36_full	0.349	2.3	ex7_m10x30_half	0.340	0.3

Table 14: Maximum Mode I SIF values for the two models, Example 7.

Model File Name	All Linear	% difference	Model File Name	All Linear	% difference
Handbook	0.388				
ex7_m10x36_full	0.423	9.0	ex7_m10x30_half	0.408	5.2

The effect of model boundaries on the computation of the SIFs can be seen from the plot of Mode I SIF, Figure 13, which shows that there is a slight reduction of the SIF at the intersection of the crack front with the symmetry surface for the half-symmetry model compared to the full pipe model. Figure 14 presents a comparison of the SIF predictions from Bergman [Ref. 4] and from FRANC3D/BES along half of the crack front.

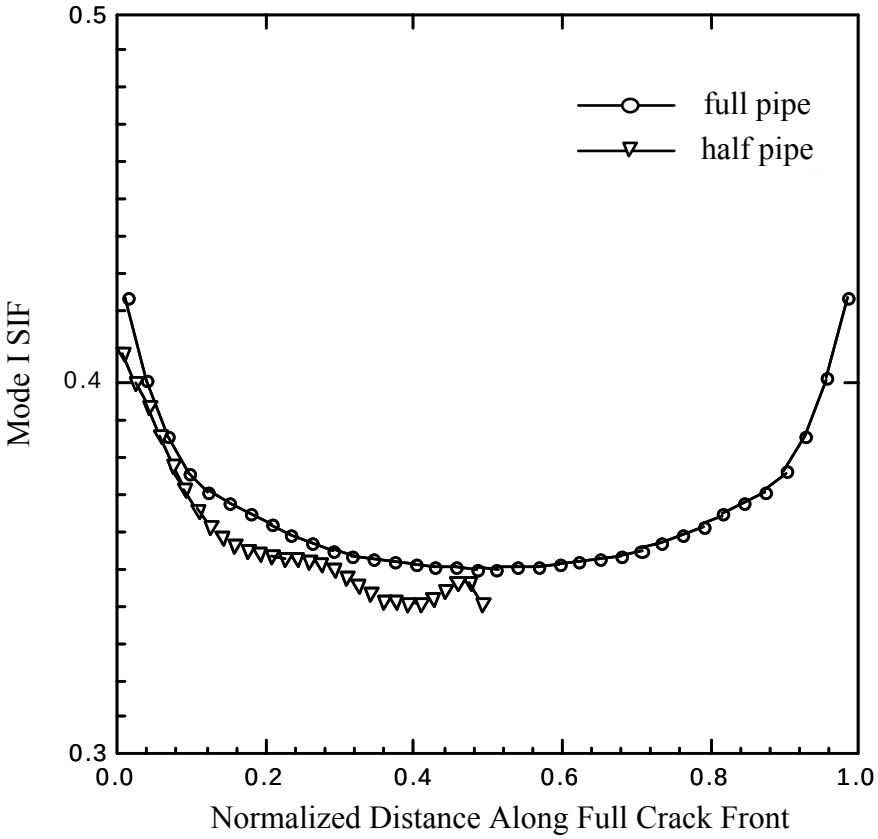

Figure 13. Example 7: Mode I SIF values along half of the crack front for the full pipe model and along the entire crack front for the half-symmetry model.

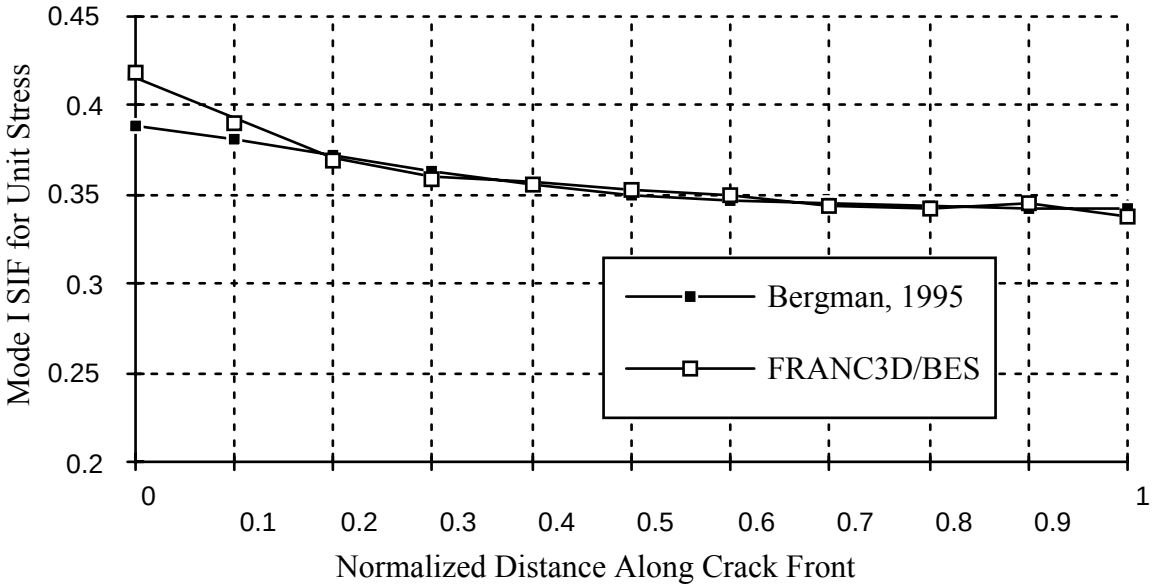

Figure 14. Example 7: Comparison between FRANC3D/BES and Bergman [Ref. 4] solution for internal circumferential surface crack in a cylinder, $R_i/t=5$, a/c=1, a/t=.4, load case 0. Half of the crack front is shown.

2.8 Example 8: Plate with Five, Flat, Part-Through Edges Cracks

Figure 15 shows a semi-infinite plate with five, part-through, edge cracks each 0.5 deep and all separated by 0.5. Two meshes are used, one with a 2x6 mesh and the other with a 4x12 mesh, Figure 14. The mesh on the free surfaces around the cracks is more refined for the second mesh due to the greater number of subdivisions. The loading on the plate is uniform tension equal to 1.0, and material properties include an elastic modulus of 10,000 and a Poisson's ratio of 0.0.

The handbook solution for Mode I SIF for the two outer edge cracks and for the middle edge crack in a finite plate with five edge cracks is given in Murakami (Ref. 3, page 114). The equations are

$$K_{IA} = F_{IA}\,\sigma\sqrt{\pi a}$$
$$K_{IB} = F_{IB}\,\sigma\sqrt{\pi a}$$

where A corresponds to the outer cracks and B corresponds to the middle crack. The correction factors are given in Murakami in the form of graphs. The separation *d* is 0.5 and the crack length *a* is 0.5, so the correction factors are

$$F_{IA} = 0.783$$
$$F_{IB} = 0.527$$

This gives a value for K_I of 0.981 for the two outer cracks and a value of 0.661 for the middle crack. These values are accurate to within 0.1%. These values are compared with those predicted by FRANC3D/BES for a fully 3D model of unit thickness. In order to avoid boundary effects as much as possible, the first and last value of stress intensity factor along the crack front are removed, and the remaining values are averaged. The results are given in Tables 15 and 16.

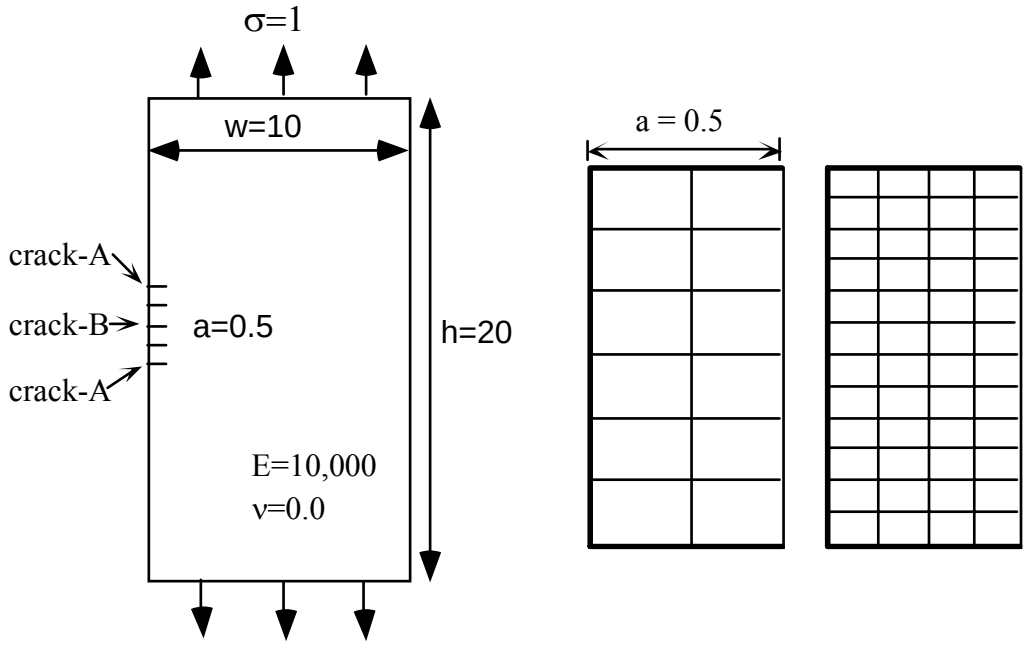

Figure 15. Example 8: Multiple (five) edge cracks in a plate under remote tension and the two meshes on the crack surfaces.

Table 15: Average Mode I SIF values for the outer crack (A) for the three meshes and the three element types, Example 8. NR indicates that the BES analysis has not been run.

Model File Name	All Linear	% error	All Quadratic	% error	Quadratic Front	% error
Handbook	**0.981**	+/- 0.1				
ex8_m2x6	0.859	12.4	NR	---	0.904	7.9
ex8_m4x12	0.923	5.9	NR	---	NR	---
ex8_m6x16	0.948	3.3	NR	---	NR	---

Table 16: Average Mode I SIF values for the middle crack (B) for the two meshes and the three element types, Example 8. NR indicates that the BES analysis has not been run.

Model File Name	All Linear	% error	All Quadratic	% error	Quadratic Front	% error
Handbook	**0.661**	+/- 0.1				
ex8_m2x6	0.449	32.1	NR	---	0.427	35.1
ex8_m4x12	0.549	16.9	NR	---	NR	---
ex8_m6x16	0.584	11.6	NR	---	NR	---

2.9 Example 9: Plate with Double, Part-Through, Flat, Edge Cracks

Figure 16 shows a finite-width plate with two, part-through, co-planar edge cracks each 0.5 units deep. Two meshes are used, one with a 2x6 mesh and the other with a 4x12 mesh, see Figure 14. The loading on the plate is uniform tension equal to 1.0, and material properties include an elastic modulus of 10,000 and a Poisson's ratio of 0.0.

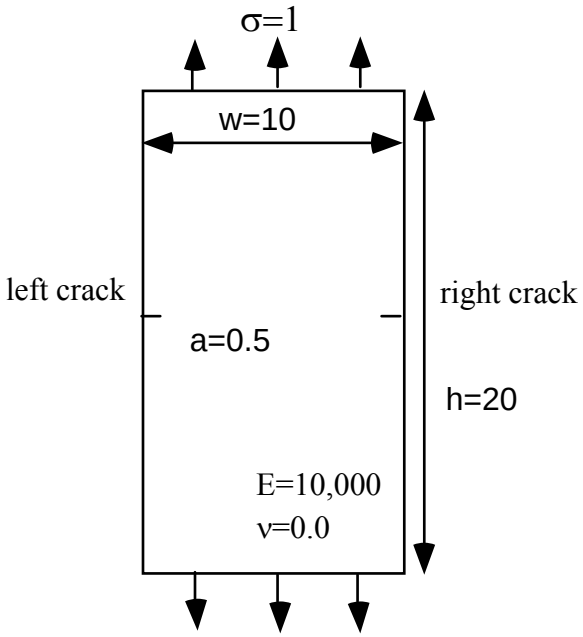

Figure 16. Example 9: Double edge cracked plate under remote tension.

The handbook solution for Mode I SIF for the two cracks is given in Murakami (Ref.3, page 6). The equations are

$$K_I = \sigma\sqrt{\pi a} \quad F_I(\alpha)$$

$$\alpha = \frac{2a}{w}$$

$$F_I(\alpha) = \left(1 + 0.122\cos^2\left(\frac{\pi\alpha}{2}\right)\sqrt{\frac{2}{\pi\alpha}\tan\frac{\pi\alpha}{2}}\right)$$

For this model, the correction factor is 1.122 and the value of Mode I SIF is 1.406, accurate to within 0.8%. The average values from the FRANC3D/BES analyses are computed by discarding the first and last values to remove the boundary effect and then averaging the remaining values. The results are given in Table 17.

Table 17: Average Mode I SIF values for two edge cracks for the three meshes and the three element types, Example 9. NR indicates that the BES analysis has not been run.

Model File Name and Crack	All Linear	% error	All Quadratic	% error	Quadratic Front	% error
Handbook	**1.406**	+/- 0.8				
ex9_m4x6_left	1.360	3.3	NR	---	NR	---
ex9_m4x6_right	1.360	3.3	NR	---	NR	---
ex9_m4x12_left	1.344	4.4	NR	---	NR	---
ex9_m4x12_right	1.344	4.4	NR	---	NR	---
ex9_m8x12_left	1.380	1.8	NR	---	NR	---
ex9_m8x12_right	1.380	1.8	NR	---	NR	---

2.10 Example 10: Plate with a Flat, Center, Through-Crack

Figure 17 shows a finite plate with center through-crack that is 2.0 long. Two meshes, one with a 8x6 grid and the other with a 16x12 grid (Figure 16), are analyzed. The loading on the plate is uniform tension equal to 1.0, and material properties include an elastic modulus of 1.0 and a Poisson's ratio of 0.3.

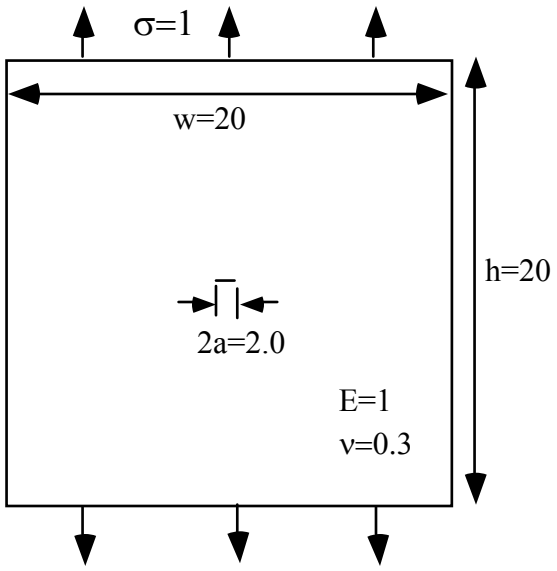

Figure 17. Example 10: Center cracked plate under remote tension.

The handbook solution for Mode I SIF for the center crack is given in Murakami (Ref. 3, page 68). The equations are

$$K_I = \sigma\sqrt{\pi a}\ \ F_I(\alpha,\beta)$$

$$\alpha = \frac{2a}{w},\ \beta = \text{ h/W}$$

For this model, the correction factor, F_1, is 1.014, and the value of Mode I SIF is 1.797, accurate to within 1.0%. The average values from the FRANC3D/BES analyses are computed by discarding the first and last values to remove the boundary effect and then averaging the remaining values. The results are given in Table 18.

Table 18: Average Mode I SIF values for the two crack fronts (left and right sides) for the two meshes, Example 10. NR indicates that the BES analysis has not been run.

Model File Name and Crack	All Linear	% error	All Quadratic	% error	Quadratic Front	% error
Handbook	**1.797**	+/- 1.0				
ex10_m8x6_left	1.825	1.6	NR	---	NR	---
ex10_m8x6_right	1.825	1.6	NR	---	NR	---
ex10_m16x12_left	1.861	3.6	NR	---	NR	---
ex10_m16x12_right	1.861	3.6	NR	---	NR	---

2.11 Example 11: Plate with a Single, Part-Through, Inclined (45 degrees), Edge Crack

Figure 18 shows a model of a semi-infinite plate with a single, part-through, inclines edge crack with a crack length of 0.5. Two meshes, one with a 8x16 and one with a 12x24 grid, are used. The loading on the plate is uniform tension equal to 1.0, and material properties include an elastic modulus of 10,000 and a Poisson's ratio of 0.0.

The handbook solution for Mode I, II, and III SIFs for an inclined edge crack in a finite plate can be computed based on the equations from Murakami (Ref 3, page 916)

$$K_I = \sigma\sqrt{\pi a}\ \ F_I(\alpha)$$
$$K_{II} = \sigma\sqrt{\pi a}\ \ F_{II}(\alpha)$$

The correction factor is given in Murakami in the form of a graph. For this model, the correction factors do not lie in the range of the graph, so the curves were extrapolated. For Mode I, the correction factor is 0.640 and for Mode II, the correction factor is 0.370. The value of K_I is then 0.810 and the value of K_{II} is 0.460. K_{III} is 0.0. The accuracy of these values is not given in the reference document.

These values are compared with those predicted by FRANC3D/BES for a fully 3D model of unit thickness. In order to avoid the boundary effects as much as possible, the first and last value of stress intensity factor along the crack front are removed and the remaining five values are averaged–six elements were used through the thickness. The results are given in Table 19.

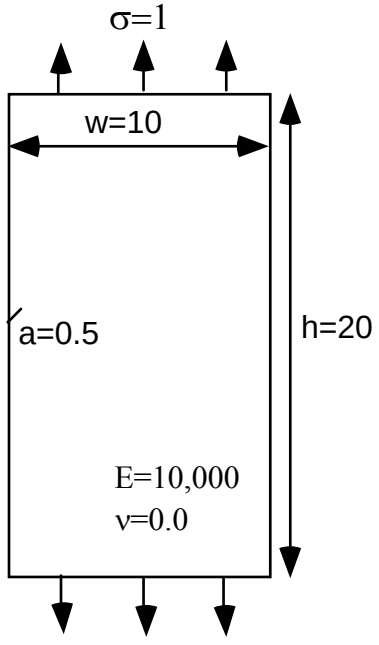

Figure 18. Example 11: Single, inclined edge crack model under remote tension.

Table 19: Average Mode I SIF values for the two meshes, Example 11.

Model File Name	Mode I SIF	% difference	Model File Name	Mode II SIF	% difference
Handbook	**0.810**		**Handbook**	**0.460**	
ex11_m8x16	0.857	5.8	ex11_m8x16	0.447	2.8
ex11_m12x24	0.852	5.2	ex11_m12x24	0.454	1.3

This problem was also analyzed in 2D using FRANC2D with 5500 degrees of freedom (DOFs) and quadratic order finite elements. Experience shows that the SIF's computed with FRANC2D with this degree of mesh refinement should be within less than 1% of the exact values. A comparison of the FRANC2D and FRANC3D/BES results is presented in Table 20. It can be seen that FRANC2D exactly matches the handbook K_{II} value, but produces a K_I that is nearly 10% higher than the handbook value. This discrepancy hints that the handbook K_I value is incorrectly low, and that the FRANC3D/BES values of K_I are less in error than suggested by Table 19.

Table 20: Comparison of 2D and average 3D Mode I SIF values, Example 11.

Model File Name	Mode I SIF	% Difference	Model File Name	Mode II SIF	% difference
FRANC2D	**0 .889**		**FRANC2D**	**0.460**	
ex11_m8x16	0.857	3.6	ex11_m8x16	0.447	2.8
ex11_m12x24	0.852	4.2	ex11_m12x24	0.454	1.3

2.12 Example 12: Plate with Two Cracks Extending From a Hole

Figure 19 shows a model of a finite plate containing a central, circular whole from which diametrically opposed straight cracks emanate. Two meshes, one with a 4x24 and one with a 6x36 grid, are used. For both meshes, quadrilateral shaped elements are used immediately adjacent to the crack front and triangular elements are used on the remainder of the crack surface. The loading on the plate is uniform tension equal to 1.0, and material properties include an elastic modulus of 10,000 and a Poisson's ratio of 0.0.

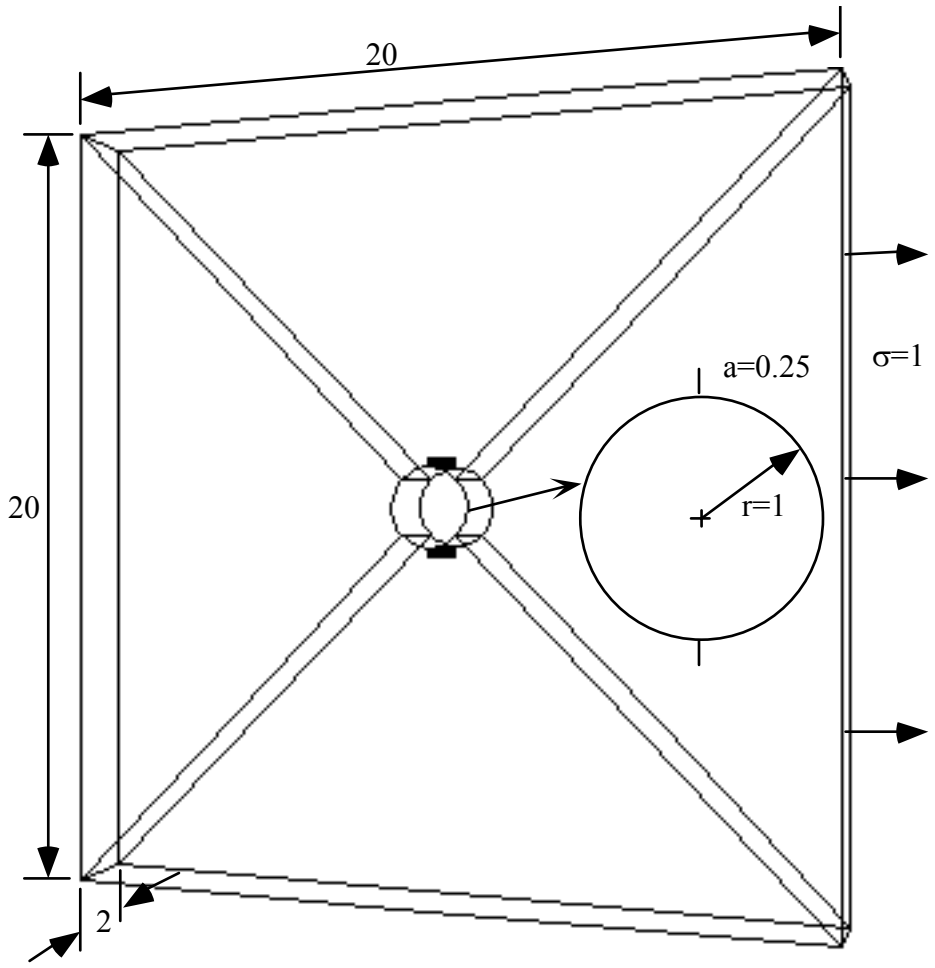

Figure 19. Example 12: Plate with a centered hole and two cracks growing from the hole.

The handbook solution is given in Murakami (Ref. 3, page 239) as,

$$K_I = F_I \sigma \sqrt{\pi a}$$

$$a = r + l$$

where r is the hole radius, l is the crack length from the hole perimeter. F_I is available from Murakami in the form of a graph and a table. For this model, a/r = 1.25, and F_I is equal to 1.017 from the table. This gives a Mode I SIF of 2.015. This result is compared to that from FRANC3D/BES in Table 21.

Table 21: Average Mode I SIF for the two cracks from the hole for the three element types, Example 12. NR indicates that the BES analysis has not been run.

Model File Name	All Linear	% difference	All Quadratic	% difference	Quadratic Front	% difference
Handbook	**2.015**					
ex12_m4x24 (upper)	2.175	7.9	NR	---	NR	---
ex12_m4x24 (lower)	2.179	8.1	NR	---	NR	---
ex12_m6x36 (upper)	2.132	5.8	NR	---	NR	---
ex12_m6x36(lower)	2.134	5.9	NR	---	NR	---

3.0 Fatigue Crack Growth Validation

The examples in Section 2 were designed to verify that FRANC3D and BES are capable of providing accurate stress intensity factors for a variety of crack geometries. With a sufficient mesh refinement, the solutions are very accurate.

Simulation of fatigue crack growth in several different structures is given in this section. Accordingly, this section concentrates on the evolving crack surface geometry, the stress intensity factor history, and the fatigue life of the structure. In some cases, there is sufficient experimental data such that the numerical results can be directly compared to experiments.

3.1 Example 13: Fatigue Crack Growth of an Elliptical Surface Crack in a Plate in Tension

Figure 20 shows a model of a Type 304 stainless steel plate containing a small, centrally located semi-elliptical surface flaw. The material properties include an elastic modulus of 210,000 MPa and a Poisson's ratio of 0.30. Both numerical (Raju and Newman, 1979) and experimental results (6,7) are available for comparison with the predictions of FRANC3D/BES. The loading on the plate is cyclic uniform tension; Figure 21 shows the load spectrum and the actual test data. Fifteen steps of crack growth simulation were performed.

Figure 22a shows the initial plate surface mesh in the vicinity of the flaw, while Figure 22b shows the mesh on the surface of the initial flaw.

3.1.1 Stress-Intensity Factor Verification

The benchmark numerical results for this problem are the finite element results reported in Raju and Newman (5). A comparison with the FRANC3D/BES results with all linear elements is given in Table 22 for K_I where the crack daylights on the free surface and for the point of deepest penetration, for the initial crack. Figure 23 compares the free surface value (the less accurate value) for the first 12 steps of propagation, before the crack breaks through the rear surface and the Raju and Newman results become invalid. This figure shows that the FRANC3D/BES results are within +/- 7% of the benchmark for all depths just short of breakthrough. The Raju and Newman results are from an equation fit to their FEM results; the values from this equation are within +/-5% of their FEM values for $a/t < 0.8$. The accuracy for depths larger than this is not known.

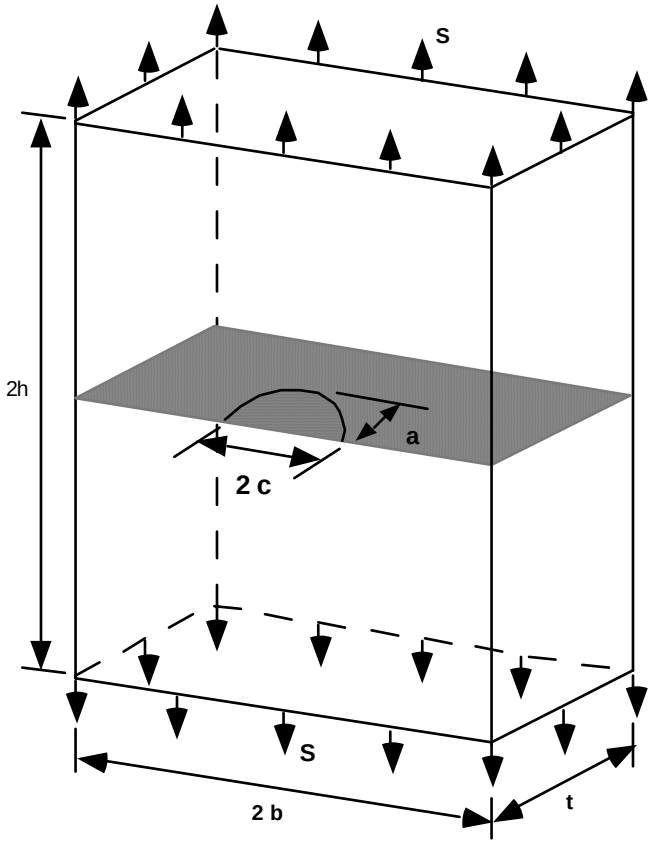

Figure 20. Example 13: Initial surface flaw in plate with a = 1.93 mm, a/c = 0.78, a/t = 0.098,
2b = 180.3 mm, t =19.75 mm, 2h >>2b.

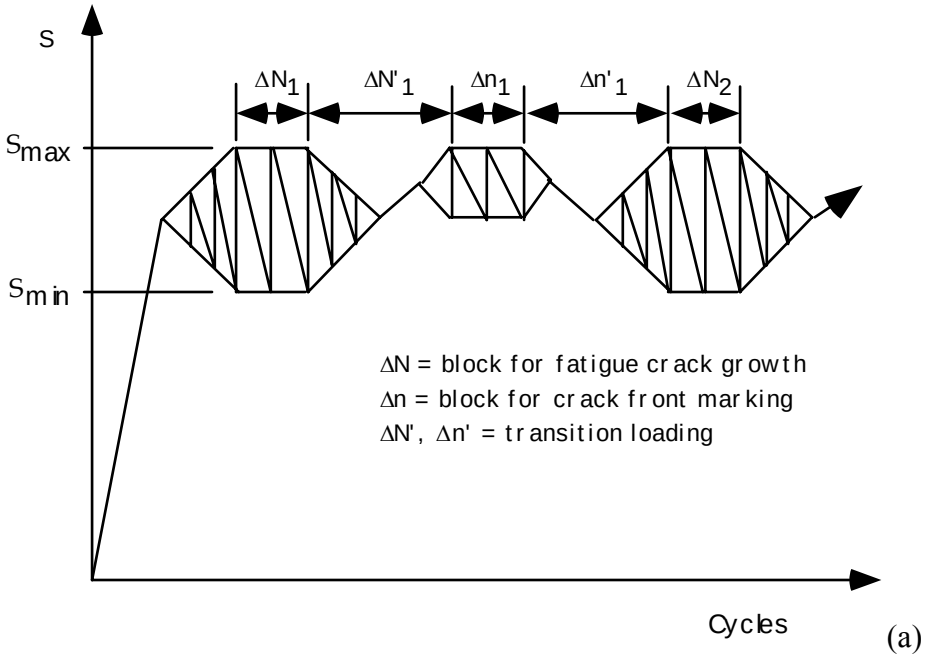

(a)

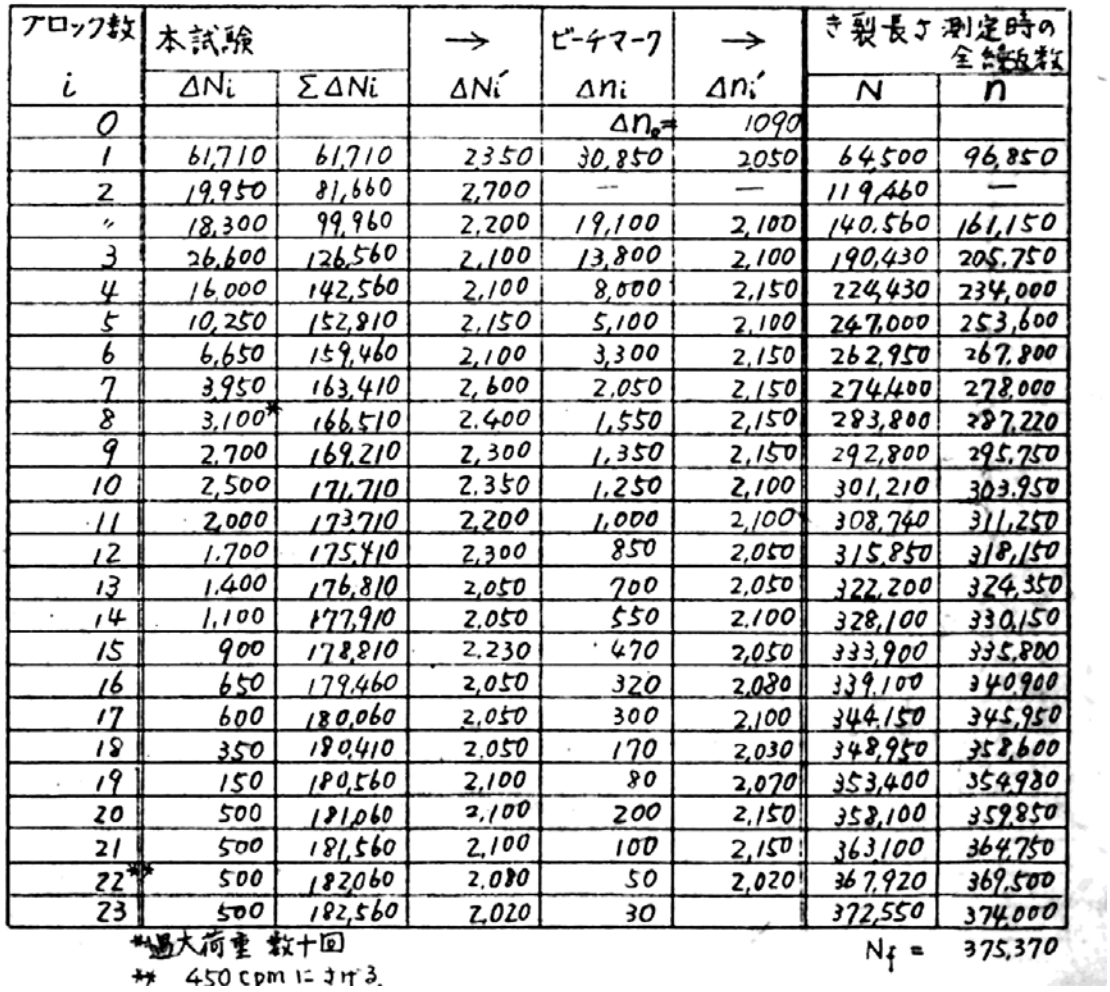

アロック数 i	本試験 ΔNi	ΣΔNi	→ ΔNi'	ビーチマーク Δni	→ Δni'	き裂長さ測定時の全繰返数 N	n
0				Δn₀=	1090		
1	61,710	61,710	2350	30,850	2050	64,500	96,850
2	19,950	81,660	2,700	--	—	119,460	—
〃	18,300	99,960	2,200	19,100	2,100	140,560	161,150
3	26,600	126,560	2,100	13,800	2,100	190,430	205,750
4	16,000	142,560	2,100	8,000	2,150	224,430	234,000
5	10,250	152,810	2,150	5,100	2,100	247,000	253,600
6	6,650	159,460	2,100	3,300	2,150	262,950	267,800
7	3,950	163,410	2,600	2,050	2,150	274,400	278,000
8	3,100*	166,510	2,400	1,550	2,150	283,800	287,220
9	2,700	169,210	2,300	1,350	2,150	292,800	295,750
10	2,500	171,710	2,350	1,250	2,100	301,210	303,950
11	2,000	173,710	2,200	1,000	2,100	308,740	311,250
12	1,700	175,410	2,300	850	2,050	315,850	318,150
13	1,400	176,810	2,050	700	2,050	322,200	324,350
14	1,100	177,910	2,050	550	2,100	328,100	330,150
15	900	178,810	2,230	470	2,050	333,900	335,800
16	650	179,460	2,050	320	2,080	339,100	340,900
17	600	180,060	2,050	300	2,100	344,150	345,950
18	350	180,410	2,050	170	2,030	348,950	358,600
19	150	180,560	2,100	80	2,070	353,400	354,980
20	500	181,060	2,100	200	2,150	358,100	359,850
21	500	181,560	2,100	100	2,150	363,100	364,750
22**	500	182,060	2,080	50	2,020	367,920	369,500
23	500	182,560	2,020	30		372,550	374,000

*過大荷重 数十回
** 450 cpm に対す3.

N_f = 375,370

(b)

Figure 21. (a) Loading spectrum used in the experiments. (b) actual test data as reported by Kawahara, Example 13.

Table 22. Comparison of K_I values at the surface and point of deepest penetration for Example 13, initial crack.

Model File Name	Surface Value (MPa√mm)	% difference	Depth Value (MPa√mm)	% difference
Reference	**445**	-	**457**	-
manu_S7-S1	460	+3.4	454	-0.65

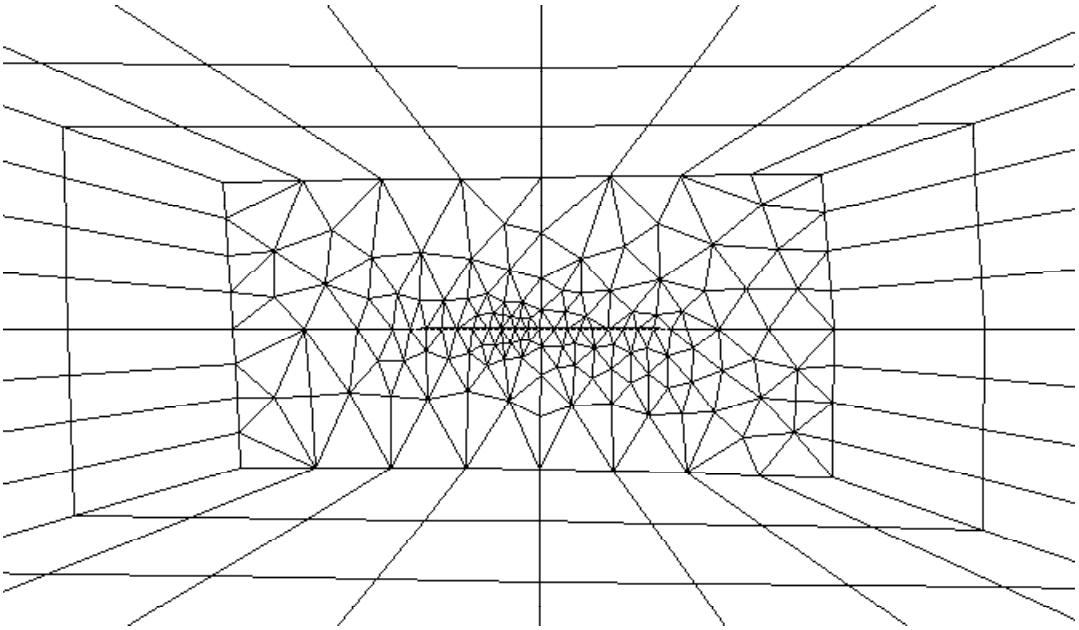

(a)

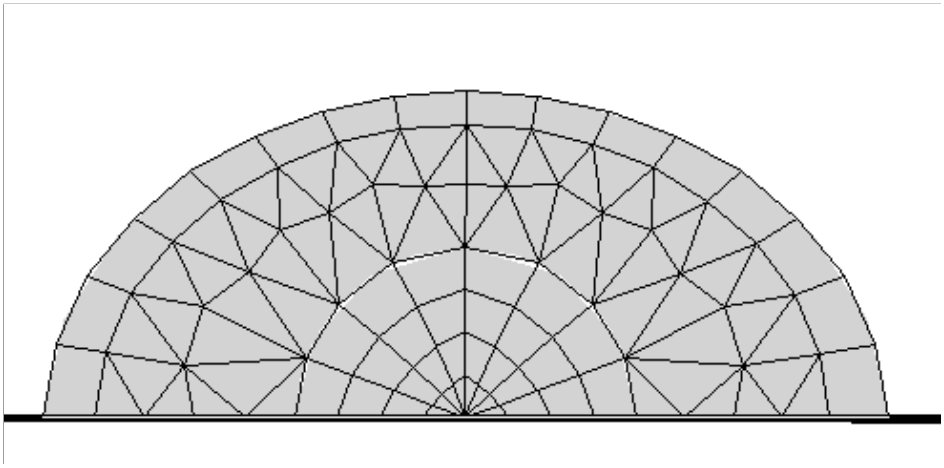

(b)

Figure 22. Mesh details for Example 13, initial crack. (a) detail around cracked surface. (b) mesh on the crack.

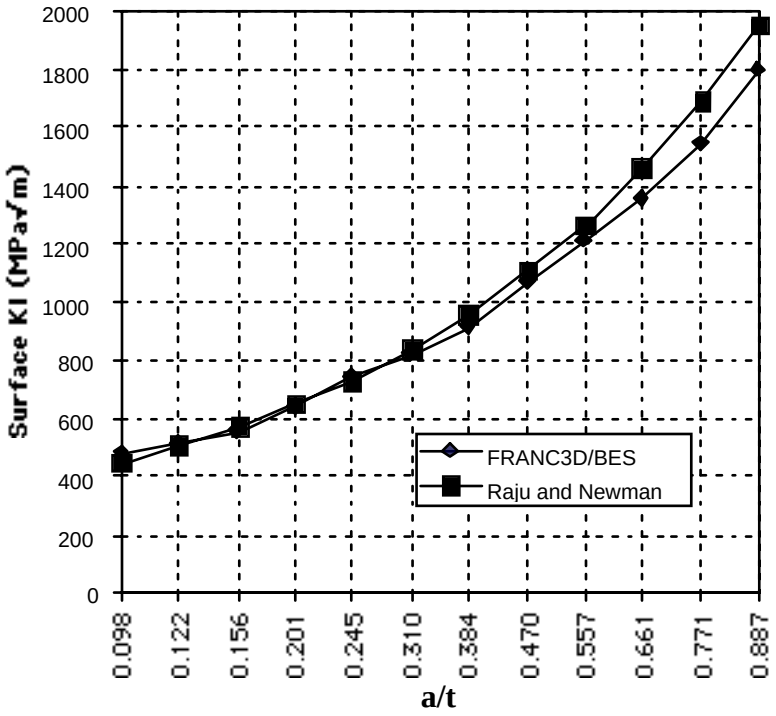

Figure 23. Compares of K_I values for the surface point for the first 12 steps of propagation, Example 13.

3.1.2 Crack Growth Rate and Shape Validation

Figure 24 shows a comparison of observed and predicted crack front shapes. A number of validation comparisons can be made with respect to these shapes and the number of cycles needed to produce them. The Paris model was used in the FRANC3D/BES predictions with C = 1.14E-15 and n = 3.85 and units of MPa and mm. These material parameters were obtained by fitting the Paris model to observed surface crack growth in the experiment being simulated. It should be noted, therefore, that any R-effect in the spectrum loading is not included in the predictions. Material parameters necessary to use the Forman-Newman-de Koning model, which does account for variable R, were not available for this example.

Surface Crack Growth:
The spectrum shown in Figure 21 had S_{max} = 245 MPa and S_{min} = 36.75 MPa, giving an R of 0.15 for the ΔN cycles, and an R of 0.575 for the Δn cycles. Four approximations of increasing accuracy with respect to the actual loading spectrum were used to create different predictions which highlight the capabilities of the Fatigue Life module in FRANC2D and the sensitivities in the results.

- Spectrum Model 1: Assume constant amplitude loading. That is, ignore all ramp and ΔN', Δn, and Δn' cycles in Figure 21(a).

- Spectrum Model 2: Bi-modal loading which includes low R, ΔN, and higher R, Δn, cycles, but ignores all Δn' cycles in Figure 21(a).

- Spectrum Model 3: Tri-modal loading which includes low R, ΔN, and higher R, Δn, cycles, but replaces all ramp ΔN' and Δn' cycles in Figure 21(a) with their average values.

- Actual Spectrum: The actual spectrum as shown in Figure 21(a) and (b).

Models 1 through 3 were readily input through the Spectrum Loads Model in FRANC3D. A small external program was written to generate the actual spectrum.

The results are presented in Table 23 with an observed surface length of approximately 28 mm as a basis for comparison.

Table 23. Comparison of Observed and Predicted Surface Crack Growth Rate: Observed to 27.7 mm, Predicted to 28 mm, Example 13.

	Total # of Cycles	% difference
OBSERVED	**359,850**	-
Predicted-Spectrum Model 1	217,000	- 39.7
Predicted-Spectrum Model 2	298,750	-17
Predicted-Spectrum Model 3	308,500	-14.3
Predicted- Actual Spectrum	385,000	7

Breakthrough:
Observed breakthrough occurred between at about 341,000 and 346,000 total cycles. The back surface half-crack length had grown to about 10.2 mm at 346,000 total cycles. Using the Actual Spectrum, FRANC3D/BES predicted breakthrough between the 12th (381,000 total cycles) and 13th (383,000 total cycles) crack increments. Predicted back surface half-crack length was predicted to be about 4.4 mm at 383,000 total cycles. Therefore, using the average of the pre-and post-breakthrough cycle counts, breakthrough was predicted to occur about 11% slower than observed.

Crack Front Shape:
Figure 24 shows that the observed and predicted crack front shapes remained approximately elliptical until breakthrough. After breakthrough, the observed through-crack developed an inflection point which was not reproduced in the predictions. This observation is consistent with the fact that observed back-surface growth rate was substantially faster than predicted; for example, at a front surface half-length of about 28 mm, observed back-surface half-length was nearly 24 mm, while the predicted back-surface half-length was about 14 mm.

Observations:
It is assuring that prediction of front-surface growth rate agreed well with observation: the Paris model material parameters were obtained directly from the observed growth rate

on the front surface. The larger difference in cycles-to-breakthrough and in crack front shape after breakthrough can be attributed to two shortcomings of the Paris model: it does not account for the variable constraint along the crack front, especially that which must occur just before and after breakthrough, and it does not account for transition effects as crack growth rate rapidly accelerates, as occurs here as the crack breaks through.

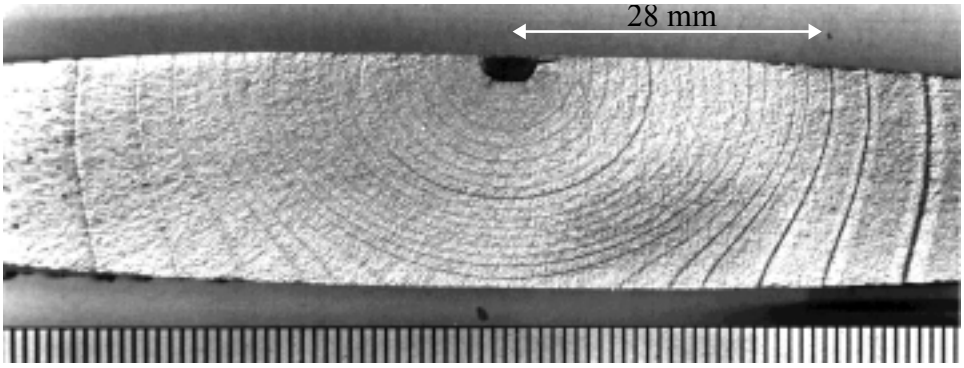

(a)

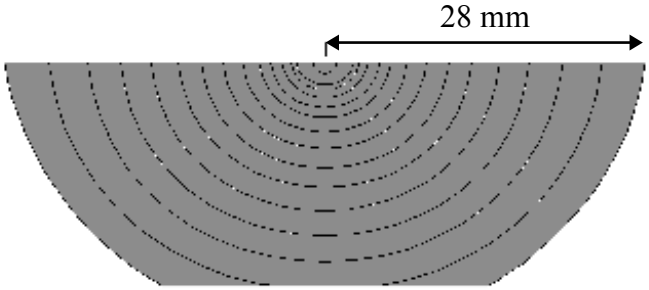

(b)

Figure 24. Comparison of observed and predicted crack front shapes: (a) observed with a front at 27.8 mm of front-surface crack growth at 359,850 cycles, (b) predicted shapes up to 28 mm of front surface crack growth, Example 13.

3.2 Example 14: Angled Elliptical Surface Crack in a Beam in Bending

The next example is a beam of 2219-T851 aluminum tested in four-point bending with an initial angled and offset half-penny shaped crack on the bottom surface, Figure 25 and Table 24. This test configuration was used by Riddell (8) to evaluate FRANC3D's capability for accurately predicting fatigue life for non-planar cracks. The initial crack radius was approximately 0.25 inches. The crack is angled 45 degrees from the beam axis and the crack center is offset from the beam center by about 0.25 inches. The beam was subjected to a constant amplitude, R= 0.214, four-point bend loading of $\Delta p = 11.54$

kips.

The initial model was meshed and boundary conditions corresponding to a unit load were applied. The model was then prepared to run automatically for 15 steps of crack growth.

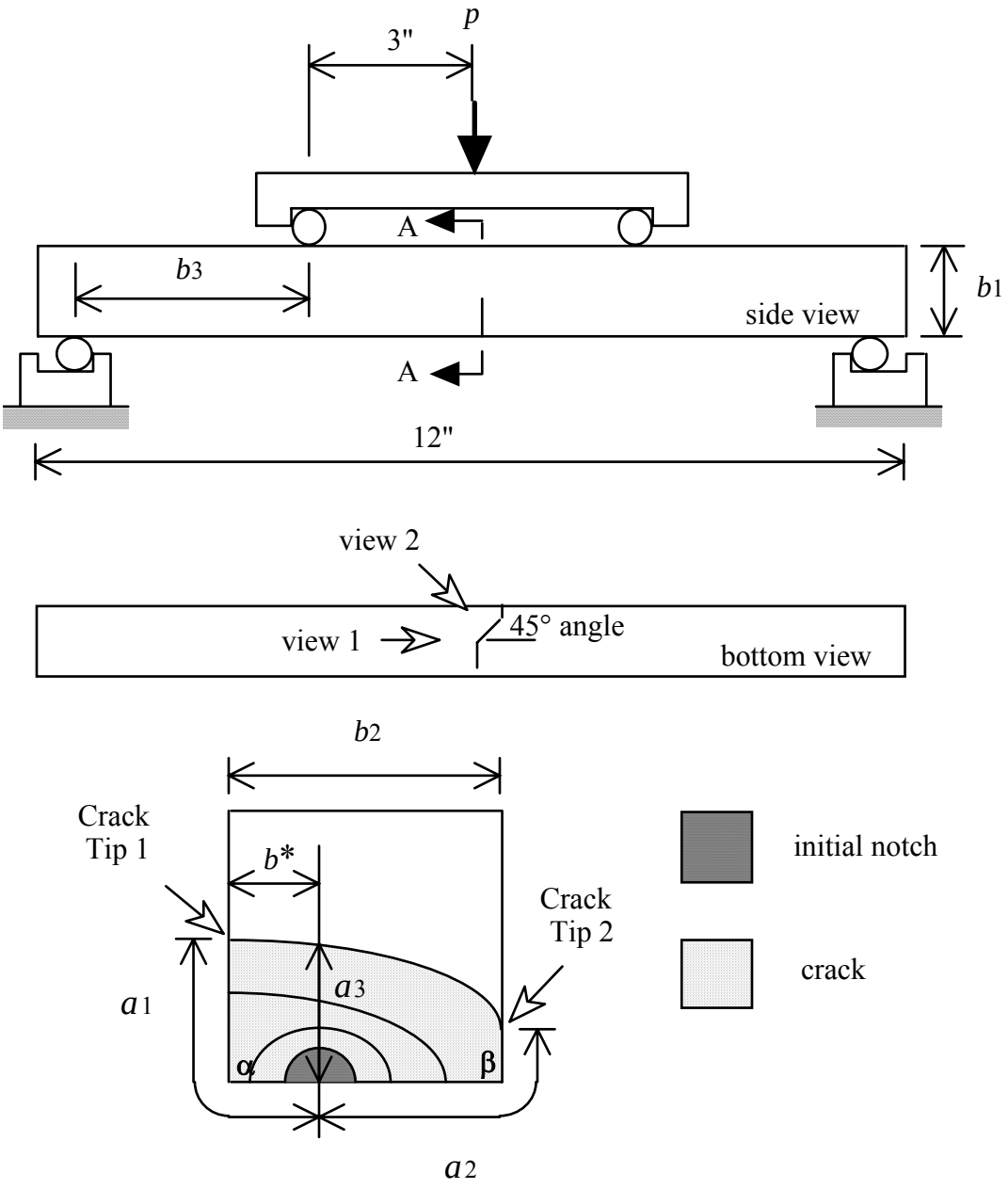

Figure 25. Beam in four-point bending with an initial angled half-penny shaped crack, Example 14. From (8).

Table 24. Testing Parameters for Example 14

Dimension	Average Value	Units
$a_1(0)$	0.184	inches
$a_2(0)$	0.184	inches
$a_3(0)$	0.250	inches
$c_1(0)$	0.174	inches
$c_2(0)$	0.174	inches
b_1	2.000	inches
b_2	1.500	inches
b_3	2.412	inches
b^*	0.508	inches
Δp	11.54	kips
R-ratio	0.214	-
l_1	106,812	cycles
l_2	171,006	cycles

Upon loading, the crack immediately begins to turn to align itself to be perpendicular to the direction of maximum tension, Figure 26. Between crack growth steps 6 and 7, the half-penny shaped crack transitions around the α-corner of the beam to become a corner crack. This happens at one side of the beam first because of the initial offset from the beam center. In this case, the numerical transition is simple and smooth because the crack front of the previous step happened to intersect exactly at the corner of the beam. This transition occurred at about 106,800 cycles in the test, Table 24.

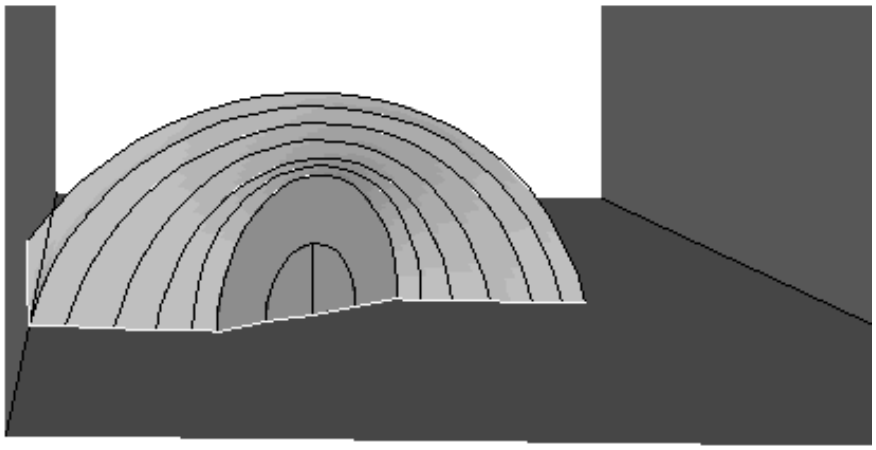

Figure 26. The angled crack turns to align itself normal to the principal tensile stress field, and eventually transitions from a half-penny surface crack to a corner crack, Example 14.

Between steps 13 and 14, the crack transitions into a part-through crack as the crack propagates around the β- corner of the beam, Figure 27. In this case, two new faces are required to represent the new crack surface in FRANC3D. An extra edge connecting the

new crack tip to the old crack front is added automatically so that two faces, each composed of four edges, are created. This transition occurred at 171,000 cycles in the test, Table 24.

Further steps of propagation allow the crack front to become essentially straight as the crack approaches the upper surface of the beam, becoming a simple part-through type of crack. The automated analysis ended at propagation step 15.

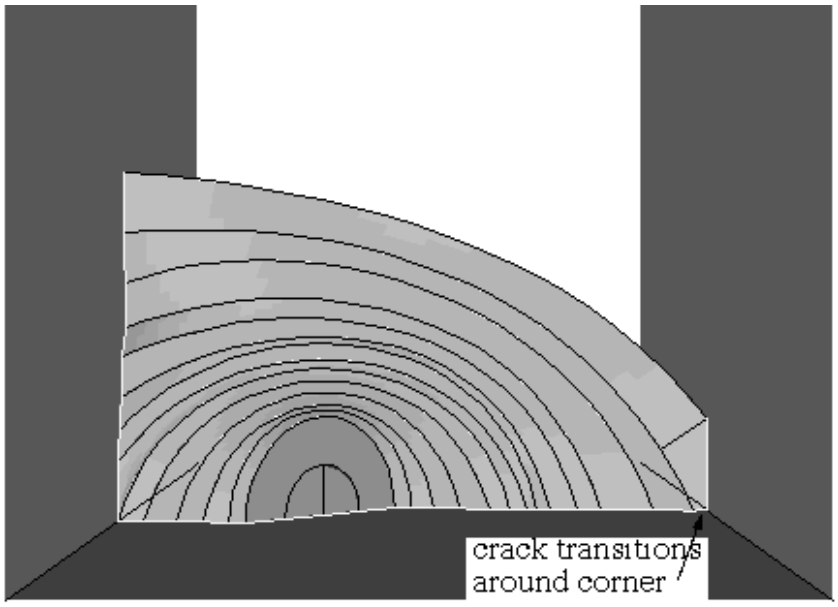

Figure 27. Final predicted crack shape. The crack has transitioned around the second corner using two geometric surfaces, Example 14.

Figure 28. Final observed crack shape. The shiny fracture surface is the fatigue crack; duller surface is fast fracture, Example 14.

Riddell (8) has compared the FRANC3D/BES simulations with experimental results in detail. Observations of crack shape, traces of crack tip locations on exterior surfaces of the beam, and fatigue life were made. The simulated final crack shape compares well with the observed final shape, Figures 27 and 28, as do the surface trace of crack tip locations, Figure 29.

A typical predicted stress intensity factor (SIF) history is shown in Figure 29. For 3D cracks, there is no single value of stress intensity factor, and therefore, there is no single stress intensity factor history. The fatigue life predictions to follow are done using different baselines for establishing a history. Further, although this problem involved mixed-mode loading, only the K_I values were used in life prediction. Predictions were based on the Paris model, with C= 1.1e-09 and n = 3.79. This C-value was adjusted for the actual R, 0.214, used in the test. The n-value was selected to produce the same crack growth rate for the Paris model as that for the Forman-Newman-de Koning model for which growth rate parameters were available for this alloy in the FRANC3D materials database.

Three events can be used as bases for comparison: arrival of the crack in the α-corner, in the β-corner, and surface lengths a_1 and a_2 for the final fatigue crack front. The comparisons are shown in Table 25. Prediction of arrival in the α-corner was significantly different from observed; this is likely due to the sharp turning of the crack which occurs between its initial front and this corner. Much more of the growth towards the β-corner is planar, and the arrival prediction at this location is very good. The last FRANC3D-predicted front used was that corresponding to the 14th automatic crack

growth step; it bracketed the observed a_1 and a_2 values.

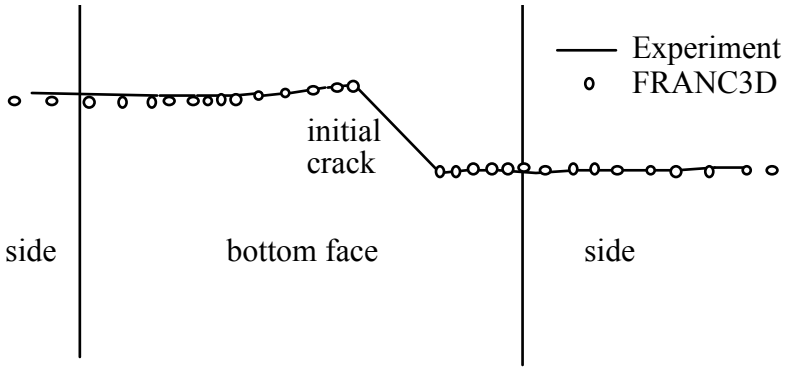

Figure 29. The crack trajectory on the exterior surfaces of the beam is well predicted by FRANC3D/BES, Example 14.

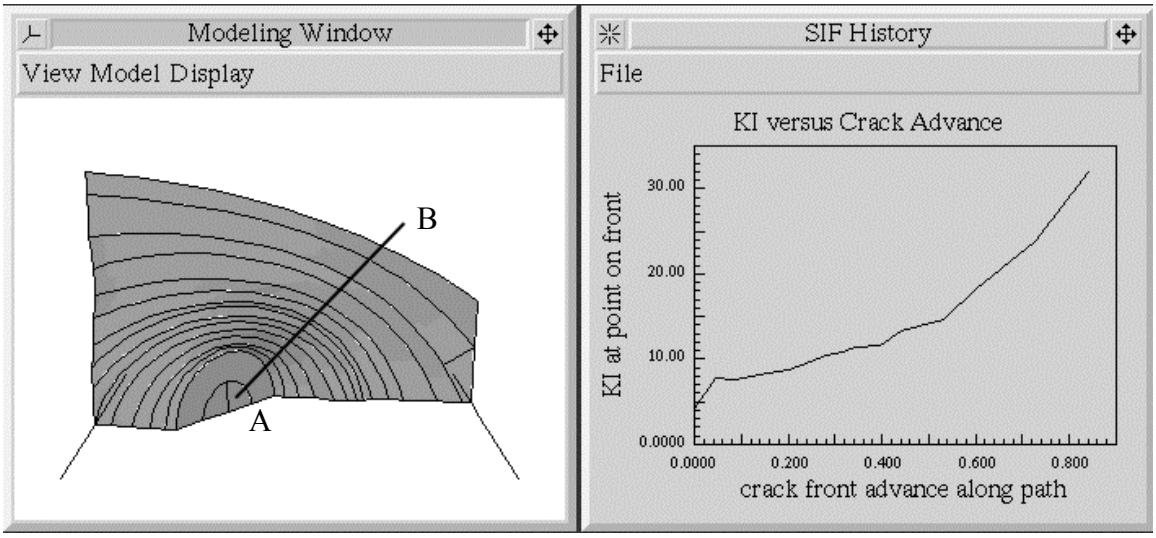

Figure 30. Typical FRANC3D-predicted stress intensity factor history for a single path (A-B) along the crack surface, Example 14.

Table 25. Comparison of Observed and Predicted Events in Example 14.

Event	**Observed**	FRANC3D/BES	% Difference
α-Corner (cycles)	**106,800**	140,000	32
β-Corner (cycles)	**171,000**	170,000	-0.5
Last Front (cycles)	**175,000**	190,000	8.5
a_1 (in.)	**1.26**	1.42	12.7
a_2 (in.)	**1.38**	1.34	-2.8

3.3 Example 15: Embedded Crack in a Welded Connection in Tension

As an example of fatigue crack growth in a welded connection, the specimen described on page 431 in Barsom and Rolfe (9), a fillet welded web-to-flange connection, was modeled. A small flaw is located within the fillet weld. To model this flaw, an internal penny-shaped crack was nucleated in the approximate location of the flaw. The material properties include an elastic modulus of 210,000 GPa and Poisson's ratio of 0.3. Uniform remote tension is applied normal to the crack surface. The crack is allowed to propagate roughly to the point indicated in Figure 14.6 of (9), going from an internal penny-shaped crack to a "three-corners" crack with three different crack front segments.

The Figures below show that FRANC3D/BES-predicted crack growth correctly captures the general shape of the observed crack. The process of going from an internal crack to a "three-corners" crack involves many steps of propagation and complicated changes in the crack geometry and topology as crack fronts intersect various surfaces of the model.

It was not possible to predict fatigue life since crack growth rate parameters were not available for the weld metal, heat affected zone, or base metal in this test.

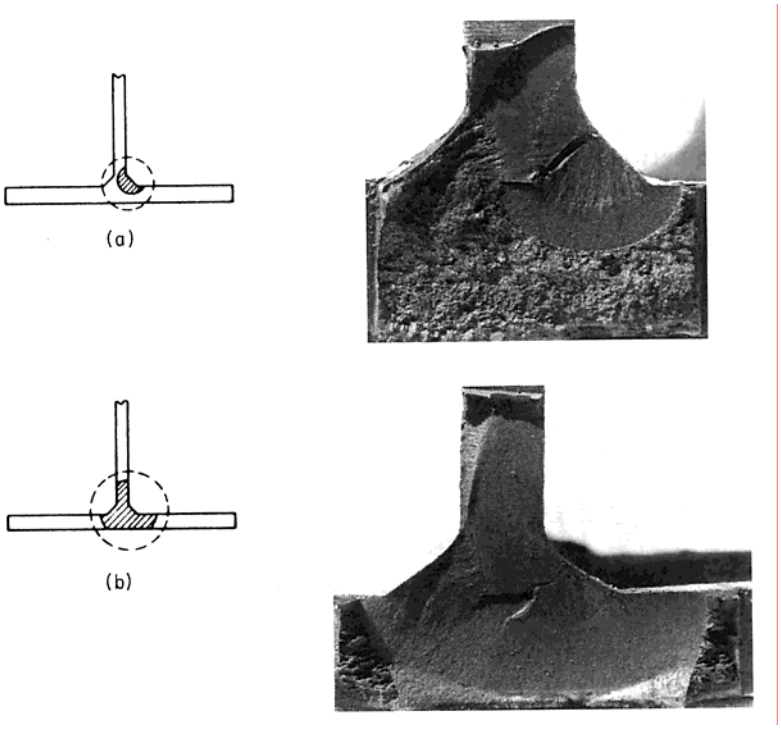

Figure 31. Photographs of fatigue crack surfaces for crack at two stages of propagation in Example 15. From Barsom and Rolfe (9).

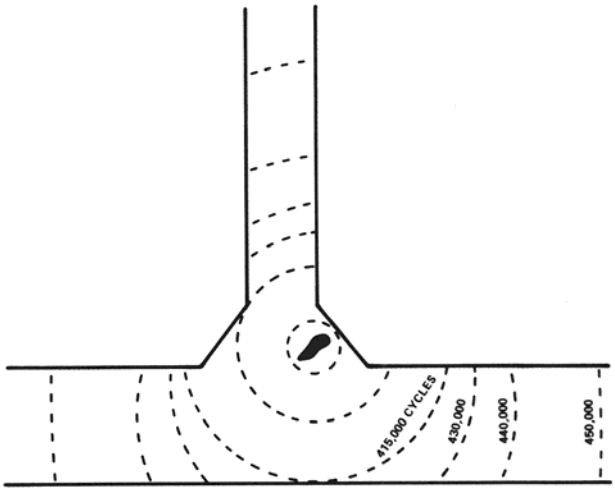

Figure 32. Observed fatigue crack growth history for Example 15. Figure 14.6 from Barsom and Rolfe (9).

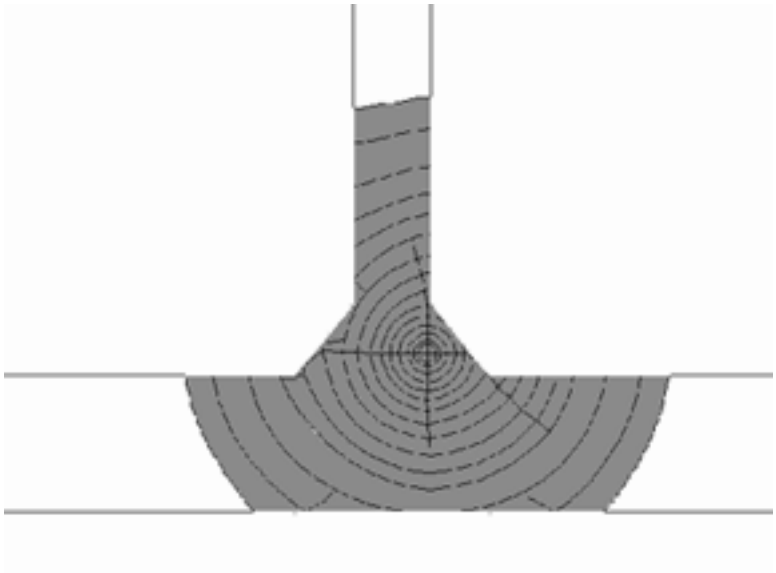

Figure 33. Predicted crack fronts for Example 15.

4 References

1. Lutz, E.D., "Numerical Methods for Hypersingular and Near-Singular Boundary Integrals in Fraction Mechanics", Ph.D. Thesis, Cornell University, 1991.

2. Chan, S.K., Tuba, I.S. and Wilson,. W.K., "On the finite element method in linear fracture mechanics", Engng. Fract. Mech., Vol 2, pp. 1-17, 1970.

3. Murakami, Y. (Editor-in-Chief), Stress Intensity Factors Handbook, Pergamon Press, 1987.

4. Bergman, M., "Stress Intensity Factors for Circumferential Surface Cracks in Pipes", Fatigue Fract. Engng. Mater. Struct., 18, 10, 1155-1172, 1995.

5. Raju, I. S., Newman, J. C., "Stress-Intensity Factors for a Wide Range of Semi-Elliptical Surface Cracks in Finite Thickness Plates", Eng. Fract. Mech., 11, 817-829, 1979.

6. Manu, C., "Three-Dimensional Finite Element Analysis of Cyclic Fatigue Crack Growth of Multiple Surface Flaws", Ph. D. Thesis, Cornell University, 1980.

7. Kawahara, M., "Study on Assessment of Afety Against Fatigue Crack Propagation in Nuclear Pressure Vessels and Piping Circuits", AFC Subcommittee, Japan Welding Engineering Society, JWES-AE-7805, 1978.

8. Riddell, W. "Experimental Validation Testing of Numerical Prediction Techniques for Three-Dimensional Fracture and Fatigue", Ph. D. Thesis, Cornell University, 1995.

9. Barsom, J., Rolfe, S., Fracture & Fatigue Control in Structures, 2nd Ed., Prentice-Hall, Inc., 1987.